Conceptual Design of Inductively Driven Long Pulsed Tokamak Reactor

（超ロングパルストカマク型核融合炉の概念設計）

山本 孝志

Conceptual Design of Inductively Driven Long Pulsed Tokamak Reactor

Conceptual Design of Inductively Driven Long Pulsed Tokamak Reactor

（超ロングパルストカマク型核融合炉の概念設計）

by

Takashi YAMAMOTO

December 1996

Department of Quantum Engineering and Systems Science,
Faculty of Engineering,
University of Tokyo

Directed by
Professor Nobuyuki Inoue
and
Associate Professor Yuichi Ogawa
and
Associate Professor Zensho Yoshida

A Dissertation
Submitted to the Division of Engineering,
the Graduate School of the University of Tokyo,
as the Partial Fulfillment for the Requirements
of the Degree of Doctor of Engineering

ACKNOWLEDGMENTS

The author's sincerest thanks to Professor Nobuyuki Inoue for his instructive advice and his hearty guidance. His continued support and a encouragement are indispensable for the accomplishment of this work.

The author's great thanks to Associate Professor Yuichi Ogawa, who has always instructed and encouraged him. This dissertation is due to his accurate advice, fruitful suggestions and constructive criticisms.

The author's great thanks to Associate Professor Zensho Yoshida for his help and the guidance throughout the study. His physics insight and valuable suggestions have benefited this work.

Great thanks are also due to IDLT Design Group: Prof. N. Inoue, Assoc. Prof. Y. Ogawa, Assoc. Prof. Z. Yoshida, Dr. Kunihiko Okano of Central Research Institute of Electric Power Industry, Dr. Haruki Murakami of Toshiba Research & Development Center, Associate Professor Akiyoshi Hatayama of Faculty of Science and Technology, Keio University. Monthly IDLT meeting has always given the instructive advice and the valuable comments to him.

The author is also deeply indebted to researchers of National Institute for Fusion Science, especially Dr. Tsugihiro Watanabe whose advice and permitting to use of his accurate magnetic codes and Dr. Nobuyoshi Ohyabu whose comments of new concepts of the divertor. Dr. Ikuo Senda of Japan Atomic Energy Research Institute also permitted to use of his neutron wall loading code.

The author would like to thanks to Dr. Wang Jifeng of Hitachi Zosen Information Systems Co., Ltd. and Mr. Ryoji Hiwatari for discussion about the plasma transport with him. The author would like to thanks to Mr. Ko Takemura for discussion about the zero-dimensional system code.

The author would like to express his delight to his colleague Mr. Kin'ichi Sasaki for

discussing and encouraging each other.

The author would like to thank to the members in Prof. N. Inoue's chair, Dr. Hitoshi Nihei, Mr. Junji Morikawa, Dr. Satoru Takeji of Japan Atomic Energy Research Institute, Mr. Hideya Nakanishi of National Institute for Fusion Science, Dr. Masayuki Watanabe of Iwate University, Dr. Shuichi Kido of Hitachi, Ltd., Mr. Youichi Sakuragi of Tokyo Electric Power Company Inc., Mr. Yoshinori Yamakoshi of Mitsubishi Heavy Industries, Ltd., Mr. Nobumichi Akiyama, Mr. Jun'ichi Miyazawa, Mr. Yasuhiko Muto of Ministry of International Trade and Industry, Mr. Michael J. Mozjetchkov, Mr. Takahiro Suzuki, Mr. Hiroaki Asakura, Mr. Shigeo Kondo, Mr. Shin'ichiro Ono, Mr. Mitsuru Hashimoto, and Mr. Teppei Hirotsu for giving precise ideas, and Ms. Emiko Kataoka of Secretary of Prof. N. Inoue for taking care of him.

Finally, the author would like to express thank for his parents. They have been supporting and understanding his study.

Tokyo, December 1996

Takashi YAMAMOTO

山本 孝志

ABSTRACT

To overcome disadvantages of the pulsed operation tokamak reactor, such as the material fatigue, the energy storage system and so on, an Inductively Driven Long pulsed Tokamak reactor (IDLT) reactor is proposed for the DEMO reactor and the commercial reactor, and a Volumetric Neutron Source (VNS) is also proposed in this thesis. IDLT reactor could be build early phase because the R&D of the non-inductive current drive is not need. In the DEMO reactor, the low neutral wall loading is stressed on the design. The material of the structure could be SUS316 which would be used International Thermonuclear Experimental Reactor (ITER). In the commercial reactor, shorter dwell time is beneficial for getting higher availability if the engineering issues are feasible and the plasma physics is reasonably acceptable. The careful design of the operation scenario is investigated of the commercial reactor. VNS is a compact irradiation machine for the compensatory the ITER weakness.

A purpose of DEMO reactor is, of course, the demonstration of the engineering feasibility as an electric power plant, where a sufficiently long pulse operation with an ignited plasma is indispensable. Giving a high priority to the early and reliable realization of a tokamak fusion reactor over the cost performance, a low wall-loading DEMO reactor is designed, based on the scientific knowledge available from ITER plasmas and advancements of the fusion nuclear technology from the near-term R&D programs. At the first step, an austenitic stainless steel, which have a plenty of experiences under the neutron irradiation in fission reactors should be employed. A slight increase of $\sim$0.5 m in major radius is sufficient for lowering the fusion power necessary to achieve an ignition plasma from 1.3 GW to 0.6 GW in ITER-relevant plasmas, yielding a remarkable reduction of the neutron wall loading down to $0.4 \sim 0.5$ MW/m^2.

For commercial IDLT reactor, zero-dimensional (0D) plasma analysis is used for investigating the sensibility of plasma parameters and estimating the plasma temperature

ramp-up time. The pulse length of IDLT reactor is estimated about 8 hours and the temperature ramp up time takes about 30 s with 40 MW auxiliary heating power. Plasma operation contour (POPCON) plot is also used for the investigation of the characteristic of the operation point and it is stable for thermal instability.

To determinate poloidal field (PF) coil position and number, the sensibility analysis of the plasma shape parameter to PF coil system is studied. The plasma with a single null configuration and the elongation of 1.7 is adopted by IDLT reactor. Using these results, the estimation of the plasma current ramp-up and ramp-down times is analyzed under the limitations, such as, the capacity of PF coil power supply system is about 1GW. The ramp-up time of the plasma current is estimated 100 s, that is, $I_p' = 0.12$ MA/s, where I_p is plasma current, and alternative current operation makes the time for re-charging the transformer shorten. The dwell time of IDLT reactor is from 7 to 10 minutes, it is enough short compared with the operation length. IDLT reactor without the power compensate system could be adaptable within the power supply network.

The advanced physics and engineerings are adopted to IDLT reactor called Advanced IDLT reactor. H factor of 2.6 and the Troyon coefficient of 4.35 are assumed the major radius of 7.5 m and the miner radius of 1.85 m. Since long pulse operation of $5 \sim 8$ hours in the daytime and of 10 hours or more during the night are available with Advanced IDLT reactor, it seems that IDLT is attractive as a load-following electric power plant, which is adaptable for a large variation of an electric power demand during the day.

In the Appendix, the Volumetric Neutron Source (VNS) has also been designed for investigating the irradiation material data. VNS is designed by the 0D system design code, and it has confirmed that its maximum of neutron wall loading is higher than 1MW/m^2. VNS is operated by the non-inductive current drive, neutral beam injection (NBI) of 60MW (1.0MeV) is needed. In the reversed shear mode, the maximum β is increased from 2.8% to 3.8% and the demand auxiliary power is decrease to NBI of 24MW (0.55MeV) with lower hybrid resonant frequency heating (LHRF) of 14.7MW.

The new object-oriented system code is also described in the Appendix. This code is worked on the workstation and/or the personal computer. The modules are distributed on the computer on the network. The modules are loosely coupled, therefore, the existing code can be fitted easily. In this chapter, the abstract of the object-orient technology is described and the software development is investigated.

In the last chapter of the Appendix, a new method for a ramp-up scenario; *i.e.*, the start-up with the small plasma surface instead of the low plasma density, is proposed with the results of the simple 0D time-dependence simulation estimated L/H transition. The auxiliary power for ramp up can be decreased by new method compared with the usual scenario. The necessary auxiliary heating power is about 50MW with new method, while 70MW with full-size start-up scenario in the ITER EDA parameter.

Contents

I Introduction **1**

1 Introduction **3**

1.1 Overview of fusion reactor 3

1.2 Review of the reactor design 5

1.2.1 STARFIRE 6

1.2.2 SSTR 7

1.2.3 ARIES, Starlite Project 7

1.2.4 DREAM 11

1.3 Review of the system code 12

1.3.1 TSC 12

1.3.2 SUPERCOIL 13

1.3.3 TORSAC 14

1.3.4 TRESCODE 14

1.3.5 ASC 15

1.3.6 SUPERCODE 15

1.4 Structure of the thesis 16

II Calculation Code **25**

2 Calculation Code for Designing the Reactor **27**

2.1 Tokamak as the complex system 27
2.2 Calculation code for designing the tokamak fusion reactors 28
2.3 0D system code and its validity 30
2.3.1 Basic plasma and coil analysis 30
2.3.2 Coil design 38
2.3.3 Neutron wall loading 40
2.3.4 The validity of 0D system code 41

III Inductively Driven Long Pulsed Tokamak (IDLT) Reactor 51

3 Introduction 53
3.1 Concepts of IDLT Reactor 53
3.1.1 Objectives of IDLT reactor 53
3.1.2 Design baseline of IDLT reactor 54
3.2 The series of IDLT reactor 55
3.2.1 The structure of this part 55
3.2.2 Parameters of IDLT reactors 56

4 IDLT DEMO reactor 64
4.1 Introduction 64
4.1.1 DEMO reactor, the next step from ITER 64
4.1.2 Object of IDLT DEMO reactor 65
4.1.3 Review of the material for DEMO reactor 66
4.1.4 The demand for the power supply on DEMO reactor 67
4.2 Basic parameter design 67
4.2.1 Basic parameter decision 67
4.2.2 0D system code, the wall loading 71

4.3 Operating scenario 71
4.3.1 Ramp-up time 71
4.3.2 Plasma equilibrium 72
4.3.3 Operating scenario 73
4.4 Engineering design 75
4.4.1 Powerflow 75
4.4.2 Simple estimation of the divertor 76
4.4.3 Simple estimation of the blanket 77
4.5 Summary 80

5 Commercial reactor 103
5.1 Introduction 103
5.2 Parameter analysis from the sawtooth-free plasma 103
5.2.1 MHD criterion from plasma current distribution 104
5.2.2 Formulas to determine the plasma parameters 105
5.2.3 Results and Summary 108
5.3 Zero-dimensional plasma analysis 109
5.3.1 Plasma parameter determination 109
5.3.2 Plasma analysis with POPCON diagram 116
5.3.3 Summary 123
5.4 Magnetics design and operation pattern 123
5.4.1 Plasma equilibrium 123
5.4.2 Operating pattern 130
5.4.3 Toroidal field coil 138
5.4.4 Summary 139
5.5 Commercial reactor with the advanced physics 140
5.5.1 Introduction 140

5.5.2 Results . . . 141
5.5.3 Summary . . . 142
5.6 Summary . . . 142

6 Discussion and conclusion for IDLT reactor **195**
6.1 Rationale of IDLT reactor . . . 195
6.1.1 The occurrence of thermal and mechanical fatigue . . . 196
6.1.2 Adaptability of the power supply network . . . 197
6.1.3 Plant efficiency . . . 199
6.1.4 Summary . . . 202
6.2 The merits and the demerits of the pulsed reactor and steady-state reactor . 202
6.2.1 The merits and the demerits of the pulsed reactor . . . 203
6.2.2 The merits and the demerits of the steady-state reactor . . . 203
6.2.3 Conclusion . . . 204

IV Conclusion **211**

7 Conclusion **213**
7.1 Discussion . . . 213
7.1.1 Rough cost estimation by the plasma cross section. . . . 213
7.1.2 Route of the fusion developments . . . 213
7.2 Conclusion . . . 214

V Appendix **219**

A Volumetric Neutron Source **221**
A.1 Introduction . . . 221

A.1.1 Requirements of the neutron radiative device . . . 221
A.1.2 The merit and the demerit of neutron irradiation devices . . . 222
A.1.3 Design principle for VNS . . . 224
A.2 0D system analysis . . . 225
A.3 Plasma equilibrium . . . 225
A.3.1 Winding method for center solenoid coil . . . 226
A.3.2 Power supply for poloidal field coil . . . 226
A.4 MHD analysis . . . 227
A.4.1 Simulation code . . . 227
A.4.2 Reversed shear mode . . . 228
A.4.3 Monotonic q profile case . . . 230
A.4.4 Reversed shear profile case . . . 231
A.5 Summary . . . 231

B Proposal of the new system code **247**
B.1 Introduction . . . 247
B.2 Object-oriented technology . . . 248
B.2.1 Object orient-oriented technology . . . 248
B.2.2 Object-oriented language . . . 252
B.2.3 Method of software development . . . 254
B.3 Implementation . . . 257
B.3.1 Objects of the system code . . . 257
B.3.2 Network distributed code . . . 257
B.4 Conclusion . . . 257

C Ramp-up Scenario with L/H Transition by Point-model Simulation **268**
C.1 Introduction . . . 268

C.2 Simulation methods 269
C.3 Results 271
C.3.1 POPCON plot and 0D simulation 271
C.3.2 Fixed-full-size ramp-up simulation 272
C.3.3 Reshaped-size ramp-up simulation 272
C.4 Conclusion 273

References **283**

List of Tables

1.1 Comparison plasma parameters of ITER EDA, STARFIRE, SSTR, ARIES-I, PULSAR-II, and DREAM. 18
1.2 Review of the system codes. 19

2.1 Yield strength and the tensile strength of the stainless steels. 42
2.2 Parameters of 0D system code. 42
2.3 Comparison with the result of 0D system code and ITER EDA. 42

3.1 Principal parameters of the series of IDLT reactor. 57
3.2 Comparison plasma parameters with other proposed reactor. 58
3.3 Parameter list of IDLT commercial reactor. 59

4.1 Parameter list of DEMO fusion reactor. 82
4.2 Consumption of IDLT DEMO reactor. 83
4.3 Operation scenario that total ramp-up phase is assumed 150 seconds. . . . 83
4.4 Maximum consumption power for PF coil system. 84
4.5 Breeding blanket of FER, SSTR, and IDLT DEMO reactor. 84

5.1 Plasma parameters determined under the sawtooth-free constrains. 144
5.2 Parameters for the different major radii. 145
5.3 H factor with various scaling law. 145
5.4 PF coil with the DN configuration. 146

5.5 PF coil with the SN configuration. 146
5.6 Marginal index versus the elongation. 147
5.7 Stored energy with the pancake winding and the layer winding. 147
5.8 Electromechanical parameters of CS coil. 147
5.9 Principle parameters of IDLT reactor. 148
5.10 Electromechanical parameters of PF coil. 148
5.11 PF coil current for the power capacity. 149
5.12 Plasma flux consumption summary. 149
5.13 Inductance matrix of the PF coil and the plasma. 150
5.14 Maximum PF coil power for each phase. 151
5.15 Operational scenario and the physics consideration. 152
5.16 Main parameter of IDLT and Advanced IDLT reactors. 153

A.1 Major parameter of ITER EDA, IDLT, and VNS. 233
A.2 Parameter list of VNS. 234

C.1 Main plasma parameters of ITER EDA. 275

List of Figures

1.1 Cross section of STARFIRE. 20
1.2 Side view of SSTR. 20
1.3 Side view of ARIES-I fusion power core. 21
1.4 Level of radioactivity as a function of time after shutdown. 22
1.5 Side view of PULSAR-I fusion power core. 23
1.6 Comparison with the reactor size of ARIES and PULSAR. 23
1.7 Component layout of DREAM tokamak. 24

2.1 Schematic view of a tokamak. 43
2.2 Tokamak as a complex system. 44
2.3 Flowchart of 0D system code. 45
2.4 Schematic plasma cross section. 46
2.5 Stress of the TF coil's can. 47
2.6 Distribution of the neutron wall load. 47
2.7 Results of the 0D system code, ITER EDA. 48
2.8 Radial build of ITER EDA by 0D system code. 49

3.1 Birdview of IDLT reactor. 62
3.2 Cross section of ITER (EDA), IDLT Reactors, VNS and SSTR. 63

4.1 Schematic scenario of fusion reactor development. 85

4.2 Critical fusion power so as to ignite a DT plasma is plotted for various aspect-ratio devices as a function of a plasma major radius. 86
4.3 Neutron wall loading is plotted for various aspect-ratio devices as a function of a plasma major radius. 87
4.4 Operation period by the inductive current drive is plotted for various aspect-ratio devices as a function of a plasma major radius. 88
4.5 Cross section of DEMO device. 89
4.6 Plasma operation contour (POPCON) plot in $\langle T \rangle$–$\langle n \rangle$ space. 90
4.7 Result of 0D system code with IDLT DEMO reactor. 91
4.8 Neutron wall loading of ITER EDA and IDLT DEMO reactor. 92
4.9 Plasma ramp-up for IDLT DEMO reactor. 93
4.10 Plasma equilibrium (layer winding). 94
4.11 Plasma equilibrium (pancake winding). 95
4.12 Power supply of PF coil and the coil current during the ramp-up phase (layer winding). 96
4.13 Power supply of PF coil and the coil current during the ramp-up phase (pancake winding). 97
4.14 Operation scenario of IDLT DEMO reactor. 98
4.15 Power flow chart in DEMO reactor. 99
4.16 Maximum temperature for austenitic stainless steel. 100
4.17 Thermal stress for austenitic stainless steel. 100
4.18 Thermal profile of the breeding blanket. 101
4.19 Non steady-state thermal analysis for the thermal cycle by FER design. . . 102
4.20 Non steady-state thermal analysis for the thermal width in the breeding blanket by FER design. 102

5.1 Flow chart to determine the plasma parameters. 154

5.2 Comparison of the plasma cross section listed in Table 5.1. 155
5.3 Schematic plasma cross section. 156
5.4 Pulse length as a function of the major radius. 157
5.5 Plasma current as a function of the major radius. 157
5.6 Magnetic flux and stored energy as a function of the major radius. 158
5.7 POPCON plot with ITER89P scaling law. 159
5.8 Radius distribution of the plasma temperature and density. 160
5.9 Dependence of the H factor by the plasma profile. 160
5.10 Trajectory for plasma temperature ramp-up in POPCON plot. 161
5.11 Auxiliary heating power necessary for ignition. 162
5.12 Inherent stable for thermal instability. 163
5.13 Contour plot of the growth rate for the thermal instability. 164
5.14 Contour plot of the growth rate for the thermal instability by the density perturbation. 165
5.15 Cross section of the IDLT plasma and the PF coil with the DN configuration. 166
5.16 Stored energy of the PF coil W_{coil} and the divertor coil current I_{div} as a function of the plasma elongation. 167
5.17 W_{coil} and I_{div} as a function of the plasma triangularity. 168
5.18 W_{coil} and I_{div} as a function of the spatial distribution of the plasma current. 169
5.19 W_{coil} and I_{div} as a function of the poloidal beta. 170
5.20 W_{coil} and I_{div} as a function of moving the magnetic axis from the center. 171
5.21 Cross section of the plasma and the PF coil with the SN configuration. . . 172
5.22 Stabilization of the vacuum vessel. 173
5.23 Plasma equilibrium with the pancake winding. 174
5.24 Plasma equilibrium with the layer winding. 175
5.25 Dependence of the electromechanics parameter by the height of the CS coil. 176

5.26 Plasma equilibrium of IDLT reactor with the SN configuration. 177
5.27 Contour plot of the error field with the height of the 10 m CS coil. 178
5.28 Contour plot of the magnetic flux. 179
5.29 Magnetic field at the maximum magnetization. 180
5.30 Magnetics flux at the maximum magnetization. 181
5.31 Schematic pattern of the plasma current and the poloidal beta. 181
5.32 Schematic pattern of the magnetic flux. 182
5.33 Schematic pattern of PF coil currents (PF#1 $\sim$ #3). 183
5.34 Schematic pattern of PF coil currents (PF#4 $\sim$ #6). 184
5.35 Shape variation of the plasma cross section during the ramp-up. 185
5.36 PF coil current waveform produced the plasma from outer side. 186
5.37 PF coil current waveform produced the plasma from inner side. 187
5.38 AC loss of the CS coil. 188
5.39 Cross section of the TF coil of IDLT reactor. 189
5.40 Toroidal magnetic field of IDLT reactor. 190
5.41 Toroidal ripple of IDLT reactor. 191
5.42 Result of 0D system code of IDLT reactor. 192
5.43 Result of 0D system code of Advanced IDLT reactor. 193
5.44 Comparison of the radial build between IDLT reactor and Advance IDLT reactor. 194

6.1 Permissible mechanical stress of toroidal coil vs. operation cycles calculated for STARFIRE. 206
6.2 Fluctuations of electric power demand. 207
6.3 Power flowchart of the fusion power plant. 208
6.4 Plant efficiency of the fusion reactor. 209

6.5 Current drive efficiencies for various techniques of non-inductive current drive. 210

7.1 Cross section of ITER (EDA), IDLT Reactors, VNS and SSTR. 216
7.2 Fusion development program. 217

A.1 Time schedule of ITER, VNS, and IDLT series. 235
A.2 Results of 0D system code for VNS. 236
A.3 Plasma equilibrium of VNS. 237
A.4 Parameter variation in the ramp-up phase. 238
A.5 Plasma equilibrium of VNS in the ramp-up phase. 239
A.6 q profile of the ordinary tokamak and the reversed shear mode. 240
A.7 MHD instability analysis by EQLAUS/ERATO codes (gauss type function). 241
A.8 MHD analysis by EQLAUS/ERATO codes (gauss type function). 242
A.9 Various parameter profile by DRIVE code (gauss type function). 243
A.10 MHD analysis by EQLAUS/ERATO codes (8 parameter type function). . 244
A.11 Various parameter profile by DRIVE code (8 parameter type function; NBI). 245
A.12 The various parameter profile by DRIVE code (8 parameter type function; NBI+LHRF). 246

B.1 Schematic of time scales and regions of applicability for fluid and kinetic simulation models in magnetic fusion. 259
B.2 Schematic of computational advances in modeling tokamak turbulence. . . 259
B.3 History of the programming language. 260
B.4 Tokamak related classes. 261
B.5 Plasma and coil related classes. 262
B.6 Core plasma related classes. 263
B.7 SOL plasma related classes. 264

B.8 Auxiliary heating, blanket and fueling system related classes. 265
B.9 Event trace diagram of the system code for the fusion reactor. 266
B.10 Schematic model of the existing system code. 267
B.11 Schematic model of the distributed-type system code which is proposed in this section. 267
C.1 H-factor f_H as a function of the threshold power P_{th}. 276
C.2 Cross section of ITER EDA plasma during the ramp-up phase and at the flattop. 276
C.3 POPCON plot for ITER EDA plasma. 277
C.4 Auxiliary heating power P_{aux} necessary for ignition. 278
C.5 POPCON plot for ITER EDA plasma at the initial phase. 279
C.6 Auxiliary heating power P_{aux} necessary for the ignition taken account of L/H and H/L transition. 280
C.7 Auxiliary heating power P_{aux} necessary for the ignition with the varying plasma surface area. 281
C.8 Excess of the heating power P_f is suppressed by the helium particle injection. 282

Part I

Introduction

Chapter 1

Introduction

1.1 Overview of fusion reactor

The importance of energy sources to the human society is fundamental [1,2]. The energy consumption in developing nations is about five times lower than ones in advanced nations. The world population is 5.5 billion at present. United Nations projections for 2060 gives a medium prediction of population doubling. Clearly the demand for energy is likely to increase by depending on the population growth and the achieved improvements in the mean standard of living.

The majority of the present energy consumption is met by burning fossil fuels. Fossil fuels are finite resource and estimated reserves correspond at present energy consumption rate to ~50 years for oil and gas, and several hundred years for coal. Very severe warnings have come from scientists who have examined the impact of continued use of fossil fuels on accumulation of CO_2 in the atmosphere and the associated greenhouse effect [3].

The only alternatives to fossil fuels are solar, fission and fusion power. These are all at the different states of the development and have very different environmental effects and perceived safety aspects. Given the magnitude of the long-term energy problem, it is clearly important to aim at diversity of supply and to develop each system to its full potential. The purpose of fusion research is therefore to explore the related science and technology and to develop prototype power-generation systems.

The basic theoretical formula covering the release of the fusion energy is the result of Einstein's special theory of relativity, $E = Mc^2$, where E is the energy, M is the equivalence of mass, c is the velocity of light. Energy release by nuclear fusion is the process maintaining the energy output of stars, such as the sun. In the sun the main energy release is through the proton-proton chain in which effectively four protons fuse to form one helium nucleus with the energy release of 26 MeV. The basic proton-proton reaction rate is far too low on the earth, fortunately there are other fusion reactions between the hydrogen isotopes, deuterium and tritium with much larger cross sections. These are:

$$D^2 + D^2 \longrightarrow He^3 + n + 3.27\text{MeV} \tag{1.1}$$

$$D^2 + D^2 \longrightarrow T^3 + H^1 + 4.03\text{MeV} \tag{1.2}$$

$$D^2 + T^3 \longrightarrow He^4 + n + 17.6\text{MeV} \tag{1.3}$$

Deuterium occurs naturally on earth in sufficient abundance to constitute an effectively infinite resource. But tritium which has half life of 12 years must be bred using the reactions between neurons and a surrounding blanket of lithium. At the temperature required for significant thermonuclear reaction rates ($> 10^8$ °K) gases are fully ionized and constitute plasmas with free electrons charge neutralized by positive plasmas. Magnetic fields can be used to confine the plasma since these restrict the particles motion perpendicular to the field.

In the late 1950s a wide range of magnetic geometries was tried, such as mirror and pinch. Confinement is however limited to the characteristic time for equilibration, at the temperatures of thermonuclear interest this rate is marginally too fast for an acceptable fusion reactor even before the influence of instabilities is included. Thus for the last decade attention has focused on so-called closed line systems, such as tokamak which a relatively strong toroidal field is added to give the required stability against gross modes of the instability. Since about 1970, the major magnetic fusion effort in the world has been

concentrated on the tokamak system.

The basic requirement for the fusion power generation is that the Lawson parameter $n\tau$ exceed 2×10^{20} s/m^3 at $T \sim 10$ keV, where n is the electron density, τ is the global energy confinement time, and T is the electron temperature, thus, the confinement time is one of the important parameters of the confined plasmas. Through the analysis of many experiments results with different devices, longer confinement time is observed when larger fusion experiments device. However, there have been no new tokamaks constructed or under construction for so many years now, in spite of several excellent proposals, because the cost is too high to construct in only one country budged. Next generation experiments continue to be caught up in the loop of design and redesign and so on.

INTOR [4] and ITER [5] are one of them, which are cooperation among some countries. Activity of the International Thermonuclear Reactor (INTOR) had done from 1981 to 1987, and activity of the International Thermonuclear Experimental Reactor (ITER) started from May 1988. The activity of ITER is conducted under the auspices of the International Atomic Energy Agency (IAEA) jointly by Euratom, Japan, the Russian Federation and the United States of America. The objectives of ITER are to demonstrate controlled ignition and extended burning of the deuterium and the tritium plasma, with steady state as an ultimate objective.

1.2 Review of the reactor design

In this section, the following conceptual design reactors are reviewed.

- In 1980', STARFIRE
- In 1990', SSTR, ARIES, PULSAR (STARLITE Project)
- Recently, DREAM

1.2.1 STARFIRE

The STARFIRE which is proposed by Argonne National Laboratory (ANL) is the first conceptual design of a commercial tokamak power plant with the cost estimation [6]. The emphasis of the study is on the simplicity of the engineering design, maintainability, lower electricity cost, and improved safety and environmental feature. The reactor has a 7 m major radius and produce 1200 MW of electric power. Figure 1.1 shows the cross section of STARFIRE and main parameter is listed in Table 1.1.

The STARFIRE operates in the steady-state operation with a lower hybrid system. The merits of the steady-state operation is the higher reliability than the pulsed operation because material fatigue is eliminated as a serious concern, the thermal energy storage is not required, the need for an intermediate coolant loops reduced. The electrical energy storage is significantly reduced or eliminated and an ohmic coils is simplified. It has been estimated that the combined benefits of steady state could be a saving in the cost of energy as large as nearly 25 % to 30 %. The cost is estimated as considered to be the tenth plant in a series of commercial reactors.

The absence of a large ohmic-heating coil permits the strategic location of equilibrium field coils and the creation of an elongated, highly triangular plasma. The most suitable equilibrium at a volume-averaged beta of 6.7 % has I_p = 10.1 MA with the current j peaked near the plasma surface.

The plasma impurity control and the exhaust system is based on the pumped limiter concept. In order to minimize the heat load to the limiter, most of the alpha-heating power to the plasma is radiated to the first wall by injecting a small amount of iodine along with the deuterium-tritium fuel system.

From the view point of the recent plasma physics, the STARFIRE cannot exist because such a optimism that Toroyon g of 7.46 is very high and iodine cannot injected the plasma. The method of cost analysis, however, has been effective to the today's conceptual reactor design.

1.2.2 SSTR

SSTR stands for Steady State Tokamak Reactor is proposed by JAERI. The SSTR is designed as a DEMO or a power reactor to be built in the near feature [7]. The main feature of the SSTR is the maximum utilization of the bootstrap current [8] in order to reduce the power required for steady state operation. This requirement leads to the choice of moderate plasma current (12 MA), high edge safety factor q_a = 5, and high poloidal beta (β_p = 2) for the device, which are archived by selecting moderate aspect ratio (A = 4) and high toroidal magnetic field (B_t = 16.5T). The bootstrap current ratio is 75%, the rest of the plasma current (25%) is driven by a high energy negative-ion-based NBI system (beam energy of 2 MeV and beam power of 60 MW) is used for the central current drive to realize steady state operation. SSTR is a single null divertor configuration to reduce magnetomotive force and the power supply capacity of the PF coils. The shallow pellet fuelling to reduce the hot neutral influx to the blanket first wall and to control the edge plasma in the H mode.

The SSTR is based on the small extension of the present physics and technologies can produce net electricity of ~1 GW if the proper physics and engineering R&D are conducted. Figure 1.2 is shown the cross section of SSTR and the main parameter is listed in Table 1.1.

1.2.3 ARIES, Starlite Project

ARIES

The study of ARIES is a US multi-institutional effort led by UCLA [9, 10]. The ARIES study is aimed at developing the several vision of tokamak power reactors with enhanced economic, safety, and environmental features. The first design, ARIES-I is a DT burning, 1000 MWe reactor. The physics basis of ARIES-I is under the consistent with ex-

isting tokamak experimental data. From the technological view point, ARIES-I makes choices that in several cases, extend beyond the present engineering achievement. In all cases, however, the technology and engineering are supported by the laboratory data and by industry trends, and it is expected that with the proper R&D, these technologies will be available within the next 20 to 30 years and could be utilized in DEMO and power reactors. In a second study, ARIES-II, the team assumes the potential advances in the plasma physics such as high plasma beta in the second MHD stable regime, that are predicted by the theory and are now establishing experimentally [11]. The ARIES team is also exploring the potential of advanced fuel cycles, specifically D-^{3}He, in the context of the ARIES-III design. ARIES-IV is also designed assume the second-stability operation, however, the blanket and shield material is different with ARIES-II [12].

A major goal for all ARIES design is to maximize the environmental and the safety attributes of fusion through innovative design and careful selection of low-activation materials. The blanket and shield are to be constructed of silicon-carbide (SiC) composite that has a low tritium inventory and the minimum induced radioactivity and the afterheat (Figure 1.4). Simultaneously, the design has a superior nuclear performance and a high coolant exit temperature (650 °C), leading to a high-efficiency Rankine-cycle power-conversion systems (49% gross).

The major parameters of the ARIES-I reactors are given in Table 1.1. The elevation view of ARIES-I is shown in Fig. 1.3. The design uses moderately high aspect ratio (A = 4.5), low plasma current (I_p = 10 MA), and high magnetic field ($\sim$ 11 T at the plasma center). Steady-state operation is presumed, based on ICRF fast-wave current drive to supplement a large (68%), theoretically predicted the bootstrap current. Impurity control and particle exhaust are based on high-recycling poloidal divertors in a double-null configuration. Self-consistent core and scrape-off-layer plasma calculations predict that with a ratio of α-particle confinement in the core to plasma energy confinement (τ_α/τ_E) of 4, the alpha exhaust efficiency is 50% and the helium ash concentration is 8%

PULSAR

The PULSAR reactor study examined the possibility of obtaining better fusion economics by using a pulsed, inductively-driven tokamak design instead of the commonly proposed steady-state, non-inductively driven tokamak designs. The operating cycle consists of a set of 2 hours burn phases separated by a 200 seconds dwell phase. During the burn phase, plasma confinement is partially sustained by an inductively-driven plasma current. The thermal output during the dwell time is compensated by the blanket and shield. The cross section of PULSAR is shown in Fig. 1.5. The blanket and shield are rather thick, they can do the storage heater in the dwell time.

PULSAR-I and PULSAR-II are 1000 MWe pulsed inductively-driven tokamak design. PULSAR-I uses a helium-cooled SiC composite as a structural material and Li_2O as a breeder [13]. PULSAR-II utilizes a blanket made of the vanadium alloy, cooled with liquid lithium. The shield is made of a mixture of the low activation austenitic steel and vanadium. The structure is made of vanadium alloy and cooled with liquid lithium [14]. The major parameters of the PULSAR-II reactors are given in Table 1.1. The reactor size comparison with ARIES and PULSAR reactors are shown in Fig. 1.6.

Starlite project

The Starlite project has evaluated the following five tokamak physics regimes as candidates to be used in conceptual design of the US Demo Power Plant by ARIES team;

1. a steady state, first stability regime similar to ARIES-I.
2. a pulsed, first stability regime similar to PULSAR.
3. a steady state, second stability regime similar to ARIES-II/IV.
4. a steady state, reversed shear tokamak.
5. a steady state, low aspect ratio tokamak.

In each area, this assessment was aimed at investigating (1) the potential to satisfy the requirements and goals, and (2) the feasibility (critical issues) and credibility (degree extrapolation required from present data base) [15].

A system assessment of the above five tokamak plasma regimes has been performed [16]. In order to provide a common basis for comparing the cost of power plants, a similar blanket and shield concept has been used which uses vanadium alloy as the structural material of the first wall, blanket, and divertor and liquid lithium as the breeder. It should be noted that it is not clear if such a design can be utilized in a spherical tokamak. In addition, a maintenance scheme for radial removal sectors is utilized. This integration sector arrangement eliminate in-vessel maintenance operations and provides a very sturdy continuous structure able to withstand large loads. Lastly, in order to minimize unscheduled interruption of plant operation, all designs operate at 90% of maximum theoretical β in order to avoid plasma disruption.

An assessment of the five tokamak physics regimes of operation was made based on the economic performance and based on the maturity of the exist tokamak data base. The first-stability pulsed-plasma and steady-state regimes are closest to present data base. On the other hand, the economic performance of pulsed-plasma operation is poor (COE is 130.2 mill/kWh). First-stability steady-state (99.7 mill/kWh) did not achieve the economic requirements for Starlite project. Starlite requirement and goal for COE are 80 mill/kWh and 65 mill/kWh, respectively. The second-stability regime has a better economic performance (92.6 mill/kWh) but experimental data base for this regime is very small. The data base for the spherical tokamaks is not mature (116.0 mill/kWh) and, in addition, many critical issues remain. The reversal-shear of operation offers the best economic performance (69.7 mill/kWh). The data base for this regime, while small, is growing rapidly. Based on the superior economic performance and the growing experimental and theoretical data base, the Starlite project has chosen the reversed-shear as the reference plasma operation

regime.

1.2.4 DREAM

In a matured stage of tokamak power plant, three major requirements of the low construction cost, the high availability operation, and the environmental safety must be realized simultaneously as the final goal. DREAM which is proposed by JAERI is stands for DRamatically EAsy Maintenance [17]. It has a new concept, an easy maintenance scheme for the high availability operation. For the easy maintenance scheme, a high aspect ratio configuration of 8 and very low activation material SiC/SiC composite are introduced. The torus system is radially divided into equal sector forms an assembling unit. Each sector of the torus system is removed horizontally in a single radial straight motion between the adjacent TF coils (Fig. 1.7). High temperature helium cooling system of 900 °C is introduced for achieving a high thermal efficiency more than 50 %.

One advantage of the high aspect ratio configuration is to enable all the piping and the feeder systems to be extracted in the torus inboard region. The relatively low plasma current of 9.2 MA and high bootstrap current fraction of 87 %, the fusion gain "Q" of more than 50 is expected. The high toroidal field of 20 T, which 14.5T on the plasma center, lead to high fusion power of 5.5 GW in spite of relatively small plasma volume (80 % of ITER plasma volume). The other plasma parameters are same as ITER. For example, MHD safety factor of 3, Troyon factor of 3 for beta limit, and the H-mode enhancement factor of 2 are used.

The activation dose of the SiC/Li_2O blanket and SiC/TiH_2/B_4H shields one day after shutdown after twenty full power years operation of the reactor has been enabled as the blanket activation dose decay by 5 orders of magnitude and the shield activation dose decay by 3 orders of magnitude. TiH_2 is very efficiently neutron shielding material. It is found that radwast from irradiated SiC/SiC composite with impurities could be disposed

be nearly the same way as the shallow land burial method presently applied to the low level waste in Japan.

1.3 Review of the system code

The following system codes are reviewed in this section.

- TSC
- SUPERCOIL
- TORSCA
- TRESCODE
- ASC
- SUPERCODE

1.3.1 TSC

The Tokamak System Code (TSC) was developed at the Fusion Engineering Design Center (FEDC) in Oak Ridge National Laboratory (ORNL) [18]. The TSC calculates the tokamak performance, the cost, and the configuration as a function of plasma and engineering parameters. It does not consider tokamak configurations that generate electrical power or incorporate breeding blankets. The code has a modular (or subroutine) structure to allow independent modeling of each major tokamak component or system. The independent modules are linked by a driver or executive routine. The geometrical configuration for the tokamak is established by starting at the plasma major radius and progressing radially inward to the ohmic heating solenoid coil and radically outward to the TF outer leg location. Certain combinations of input parameters will result in a configuration that has inadequate radial space between the plasma and the machine centerline to accommodate all the tokamak components, in which case an error message is printed and the run is terminated. The independent modules are following; Physics module, Torus module, Toroidal

field coil module, Poloidal field coil module, Inductance module, Flux linkage module, Plasma heating systems, Neutron Beam/TF coil interface, Poloidal field power conversion module, Reactor cell, Torus vacuum module, Tritium processing module, Fueling system module, TF power conversion module, Facilities module, Heat transport module, AC power module, Instrumentation and control module, Maintenance equipment module, and Cost module.

1.3.2 SUPERCOIL

SUPERCOIL is a code for the computational design of tokamaks, including in particular ignited next-generation devices developed at Max-Planck-Institut für Plasmaphysik. It takes into account all physics, technical and geometrical constraints relevant to the basic design of a tokamak. Among the solutions of the model equations that meet all constrains the one optimized with respect to a prescribed figure of merit (typically capital cost) is determined [19]. To find the optimized point, the input parameters are divided two group, "fixed parameters" and "grid parameters". The majority of fixed parameters describe basic design characteristics. Typical examples are the blanket and shield attention lengths or the parameters characterizing the coil conductors. The remain independent parameters ("grid parameters") are self-consistently determined. In the SUPERCOIL, plasma minor radius, plasma aspect ratio, shield thickness, and magnetic field on axis are grid parameters. Once a combination of grid variables is specified, a consistent solution of the model is obtained by solving the whole set of model equations. A unique solution is found by determining that combination of input parameters that in addition minimizes or maximizes a prescribed figure of merit, typically the cost of a machine. The Next European Tokamak (NET) is studied in Ref. [19].

1.3.3 TORSAC

The TOkamak Reactor System Analysis Code "TORSAC" is developed by Japan Atomic Energy Research Institute (JAERI) in order to assess the impact of the design choices on reactor systems and to improve tokamak designs in wide parameter range [20]. This code has

1. Systematic sensitivity analysis for a set of given design parameters.
2. Cost calculation of a new reactor concept designed automatically as a result of systematic sensibility analysis.

This code is used for INTOR [21], Fusion Engineering Reactor (FER), and Swimming Pool Type Tokamak Reactor (SPTR) which is sinked in the huge pool for the shield instead of the soil shield structure proposed by JAERI [22, 23].

1.3.4 TRESCODE

The Tokamak REactor System COnceptual Design Code (TRESCODE) is also developed at JAERI on the basis of FER design studies [24]. There are two objects for this code. The first object is that TRESCODE can be applied to the parametric studies for various reactor concepts. In this objects, relative cost estimations in terms of volume, weight, input and output energy can be carried out under the design driver, constraints of the physics and the engineerings. The second object is that TRESCODE can be used for the engineering design of the tokamak core structure for the selected reactor concept. In this object, accurate radial-build and vertical-build based on the shield calculation, stress and strain analysis of magnet system can be carried out under the design constraints and conditions. Operation scenario is included with the plasma equilibrium and the poloidal field calculations to obtain the desired reactor concept.

1.3.5 ASC

The ARIES system code (ASC) analyzes the tokamak fusion power plants under given condition of plasma parameters and engineering guidelines, and estimates the cost of electricity (COE) based on the cost of each component in the fusion power plant [25]. In addition, the optimum machine size, which gives the minimum COE value, is automatically determined by the major radius at a fixed aspect ratio. Central to the ASC is a zero-dimensional, steady-state plasma-power-balance model that includes separate ion and electron energy balance, particle continuity, a specified impurity fraction, charge balance, and a β constraint [26]. The development group is in University of California, Los Angels (UCLA), Argonne National Laboratory (ANL), General Atomics (GA), and others. The main target of ASC is the Starlite project. The Starlite project has evaluated the several tokamak physics regimes as candidate to be used in a conceptual design of the US Demo Power Plant as described in Sec. 1.2.3 [27]. ASC also used to estimate the COE of the IDLT reactors and comparison with PULSAR-II [28].

1.3.6 SuperCode

The SuperCode is developed to fill the gap between currently available zero dimensional system codes and highly sophisticated, multidimensional plasma performance codes [29]. The SuperCode upgrades the reliability and accuracy of system codes by calculating the self consistent 1 1/2 dimension plasma evolution in a realistic engineering environment. By a combination of variational techniques and the careful formation there is only a modest increase in CPU time over 0-D runs, thereby making the SuperCode suitable for use as a system studies tool. The SuperCode is written by C++ language to enhance the flexibility of the programming [30], and user-friendly by using graphical user interface (GUI) [31]. The SuperCode is developed at the MIT plasma fusion center at first and later Lawrence Livermore National Laboratory (LLNL), Oak Ridge National

Laboratory (ORNL) and other sites are joined the development group for SUPERCODE . This code used for the study of ITER-like tokamak [32] and the wide range of parameter survey on the several different class of tokamak reactors, that designs are optimized in terms of COE [33].

1.4 Structure of the thesis

The organization of the thesis is as follows: In Part II, the simulation code for tokamak fusion reactor is described. Many codes are used for designing the reactor because tokamak fusion reactor is very complex system. The brief explanation about the tokamak fusion system and the codes is described. The detail of 0D system code is explicated.

Part III, The Inductively Driven Long pulsed Tokamak (IDLT) reactor is designed. The concept and philosophy of IDLT reactor are described in Chapter 3. Two type of IDLT reactor are designed in this part, a DEMO reactor and a commercial reactor. The DEMO reactor is the next step after the experimental reactor such as ITER. The IDLT DEMO reactor is designed with the stress on the low neutron wall loading in Chapter 4. The first wall is made by SUS316 which would be also used ITER. The commercial reactor is designed two type. One is designed based on the conventional physics and the technology and another is designed the advanced physics such as supporting the very high confinement mode in Chapter 5. The conventional commercial reactor is designed the first of the IDLT tokamak series [34]. The advanced commercial reactor is also studied to know that how compact the reactor with the advanced physics in comparison with conventional one. The conclusion of IDLT reactor series is in Chapter 6. The IDLT reactor overcome the demerits of the pulsed reactor, *i.e.*, the fatigue and the dwell time, by making the pulse length very long (several hours). The rationale of realizing the IDLT reactor is described. The merit and demerit of pulsed reactor is also discussed here.

In Part IV, *i.e.*, Chapter 7 is the conclusion of this thesis.

Appendix A is described about the volumetric neutron source (VNS). VNS is a material test device to accomplish the selection of the material and the blanket for DEMO. The overview of neutron test facilities and why VNS needs albeit ITER will be there is in this chapter. In this chapter, the design of VNS with plasma equilibrium, MHD instability analysis, and non-induct current drive are investigated. We also attempt the reversed shear mode to enhance the reactor ability to get the high wall loading.

Appendix B is described about proposing the new-type system code. It is a distribute, network-oriented code. Each code is run on the each machine connected to the network and communicate the input and the output date each other. The grain of the software is very large. It could be fast calculation more than one machine.

Appendix C is described about L/H transition during the ramp-up phase. The plasma ramp-up is simulated by point model with L/H transition. The used parameter for simulation is ITER EDA. The new method for lower auxiliary heating is estimated in this chapter.

Table 1.1: Comparison plasma parameters of ITER EDA, STARFIRE, SSTR, ARIES-I, PULSAR-II, and DREAM.

	ITER (EDA)	STARFIRE	SSTR	ARIES-I	PULSAR-II	DREAM
plasma major radius R [m]	7.7	7.0	7.0	6.75	7.91	16
plasma major radius a [m]	3.0	1.94	1.7	1.5	1.98	2
aspect ratio A	2.56	3.6	4.0	4.5	4.0	8
elongation κ	1.6	1.6	1.85	1.8	1.6	1.3
triangularity δ	~0.3	~0.5	~0.5	~0.2	0.35	0.1
plasma volume V [m^3]	2189	832	760	540	840	1642
flux safety factor q_Ψ	~2.85	3.4	5.0	4.5	3.54	3.0
plasma current I_p [MA]	24	10.1	12.0	10.2	13.4	9.2
bootstrap current fraction	0.21	–	0.75	0.68	0.37	0.87
plasma temperature $\langle T \rangle$ [keV]	13	17	17	20	14	14
electron density $\langle n \rangle$ [10^{20}m^{-3}]	1.07	1.2	1.4	1.5	1.03	1.7
average toroidal beta β [%]	4.2	6.7	2.7	2.0	2.8	1.0
max. toroidal field $B_{t\,max}$ [T]	12.8	11.1	16.5	21	12.5	20
toroidal field on axis B_t [T]	5.7	5.8	9.0	11.3	7.31	14.5
heating method	NBI, *etc.*	LHRF	N-NBI	ICRF	Inductive	NBI
heating/C. D. power [MW]	50	63	60	100	–	50
fusion power output [MW]	1500	3490	3000	2544	1830	5500
power multiplication	~40	~10	50	~20	>500	>50
operation time	~0.28hrs	steady-state	steady-state	steady-state	2.5 hours	steady-state

Table 1.2: Review of the system codes.

code	organization	main target	Ref.
TSC	ORNL	–	[18]
SUPERCOIL	IPP	NET, ASDEX-U	[19]
TORSAC	JAERI	FER, INTOR	[20]
TRESCODE	JAERI	FER	[24]
ASC	UCSD, *etc.*	ARIES-I	[25]
SUPERCODE	LLNL, ORNL, *etc.*	TPX, ITER	[29]

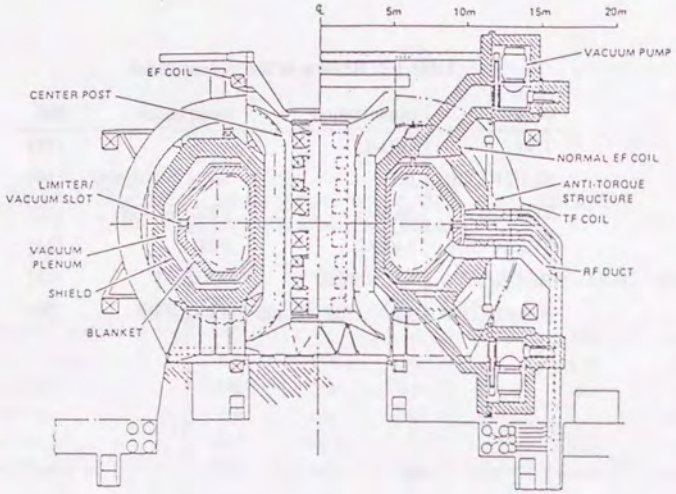

Figure 1.1: Cross section of STARFIRE [6].

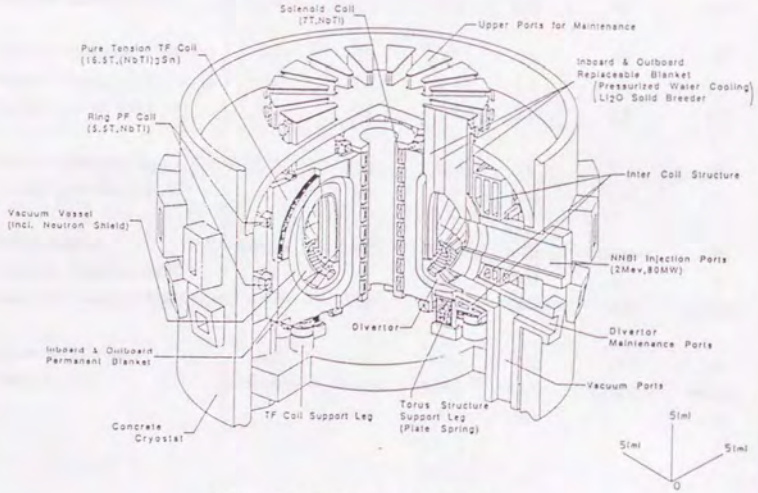

Figure 1.2: Side view of SSTR [7].

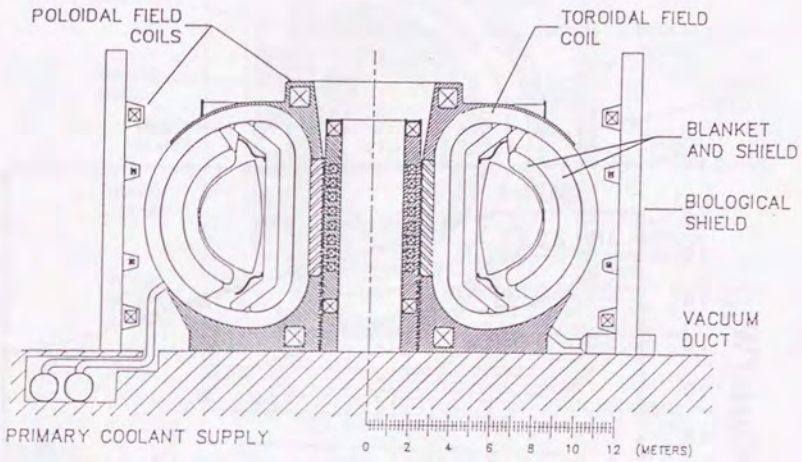

Figure 1.3: Side view of ARIES-I fusion power core [7].

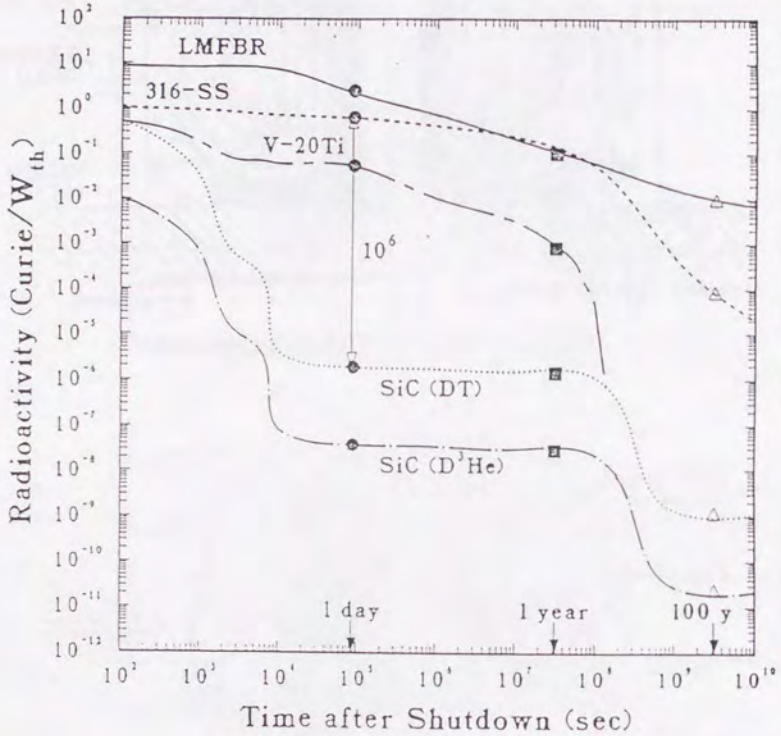

Figure 1.4: Level of radioactivity as a function of time after shutdown in fusion reactors for different potential structural materials. The fuel cycle is assumed to be deuterium-tritium (DT). For comparison, radioactivity levels after shutdown are also given for an liquid metal fast breeder reactor (LMFBR). Even at one day after shutdown the radioactivity in a low activation (SiC) DT fusion reactor is roughly one millionth of the radioactivity from a fission reactor [9].

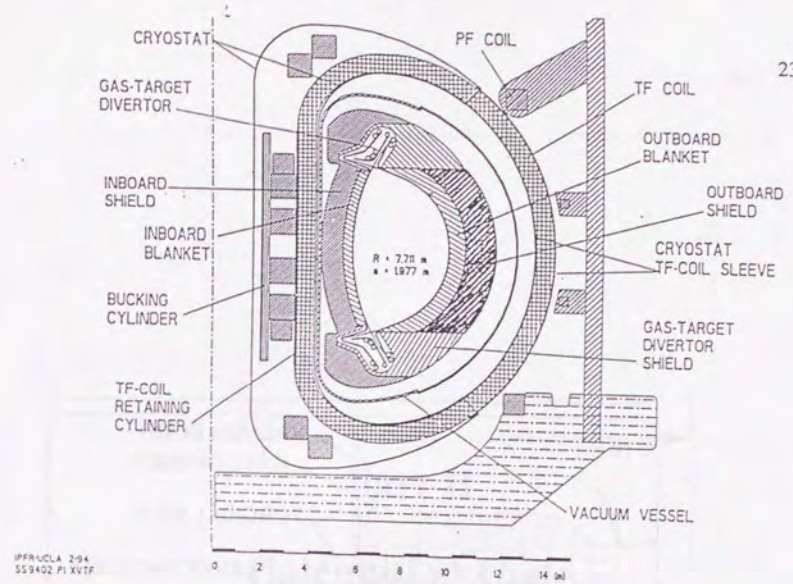

Figure 1.5: Side view of PULSAR-I fusion power core.

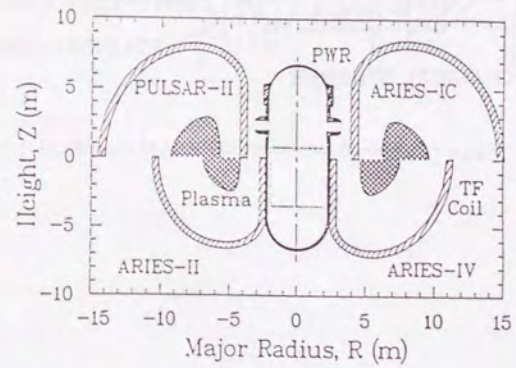

Figure 1.6: Comparison with the reactor size of ARIES and PULSAR. The fission reactor (PWR) is also shown in this figure.

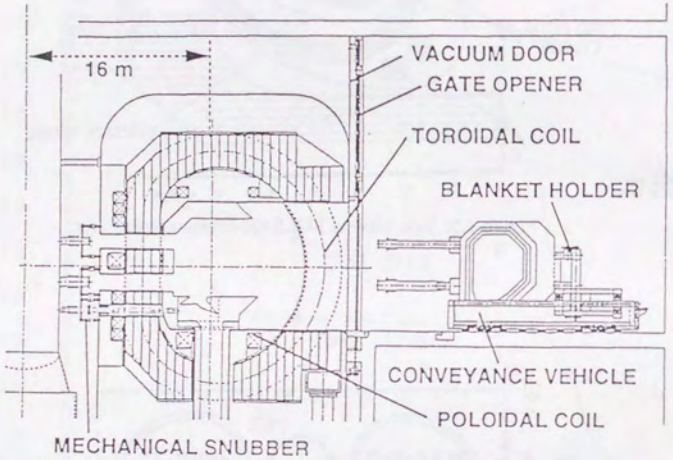

Figure 1.7: Component layout of DREAM tokamak [17].

Part II

Calculation Code

Chapter 2

Calculation Code for Designing the Reactor

2.1 Tokamak as the complex system

The tokamak is a toroidal magnetic confinement system. It was first proposed independently in the early 1950s by Igor E.Tamm and Andrei D. Sakharov and Lyman Spitzer. It has been the most promising and well developed concept in the magnetically controlled fusion research [35–37].

The schematic figure of a tokamak is shown in Fig. 2.1. The tokamak magnetic configuration is consisted of three components. The main component of the magnetic field, so-called toroidal field, is produced by toroidal field coils surrounding the vacuum vessel (blue D-shaped rings coil in this figure). The toroidal field in the center of plasma (pink doughnut) is typically of the order of several teslas by present technology, and such an toroidal field is required to suppress the magnetohydrodynamics (MHD) instabilities. The second component of the magnetic field, so-called the poloidal field, is generated by a toroidal plasma current. The most efficient method to generate the plasma current and to maintain it is to use the transformer principle with a powerful central solenoid (yellow cylinder) as the primary winding and with the plasma acting as a one-turn secondary winding. Also the plasma current provide the ohmic heating to the plasma. The combination

of the poloidal field with toroidal field lead to the helical magnetic field lines that form a set of magnetic surfaces and keep the plasma away from the vessel walls. The third component of the magnetic field, so-called the vertical field, is produced by a set of poloidal field coils (orange rings), which is used to shape and stabilize the position of the plasma.

Tokamak fusion reactor is very complex system. For example, to sustain the plasma burning, external magnet coil, fuel inject system, auxiliary heating system, vacuum system, the refrigerator for superconducting coils and others are needed. The plasma consists of a main plasma and a scrape of layer (SOL) plasma; the main plasma consists of a particles and the plasma current which is composed by inductive current, non-inductive current and bootstrap current. Each component is important for the tokamak system. One example which is dissolved the tokamak system is show in Fig. 2.2.

The each device is not independent. Each portion has an important effect on the other portions. When the magnet field of poloidal field (PF) coil is varied, then the plasma position or the plasma shape is modified. The heat from the plasma to the first wall and the divertor is changed, the pump of the divertor is effected. The refrigerator of the PF coil is affected by changing the current which makes the the magnet field of PF coil. Of course, the plasma physics such as the confinement of the energy and the particle, *i.e.*, the transport of the particle and the thermal, also changed. To keep the plasma status constant, the field of PF coil is control by a feedback system which is consisted of the magnetic prove to detect the variant field and the computer system. The fuel system and the auxiliary heating system also the part of the feedback system.

2.2 Calculation code for designing the tokamak fusion reactors

The brief descriptions of the codes used for designing the reactor are explained. Most of code is already accomplished, some codes are converted to out laboratory's computer,

some codes are modified for this thesis. 0D system code was constructed from scratch.

0D system code [38] Before using the high dimensional elaborate code, this code check the criterion, such as the stress of poloidal field (TF) coil and center solenoid (CS) coil, the flux made by CS coil for ramp-up consumption and others. The output are the elevation view of the plasma, TF coil, CS coil and bucking cylinder, ground view, radial build, and neutron wall loading [39].

3D magnetic field code: MGFLD [40] This code produce the 3D magnetic field with high precision. For example, it is used for the validation of TF coil ripple on the plasma surface. The coil shape is settled from any combination by the rectangular element and the arc element.

2D tokamak plasma equilibrium code: EQUCIR [41–43] The PF coil currents for the plasma equilibrium are produced when a plasma size and shape is specified. The PF coil position is determined to minimize the stored energy of PF coil. The demand value of power supply for PF coil is calculated by simulating the plasma ramp-up, that is calculate the plasma equilibrium at each time step.

Plasma stability analysis code: ERATO [44,45] This code analysis the MHD instability by the energy principle. The Mercier criterion, ballooning mode, and kink mode can be examined. The critical beta (the maximal beta value of the plasma which stables these instability) is determined by changing the pressure profile and the current profile. This code is combined 2D plasma equilibrium code EQLAUS for this study.

Eddy current analysis code: EDDYTOR [46] The eddy current on the shell which comes from the movement of the plasma is produced. From the distribution of the eddy current, the vertical instability can be investigated.

Plasma non-inductive current drive code: DRIVER [47,48] The current profile driven by non-inductive drive such as neutral beam injection (NBI) and lower hybrid reso-

nant frequency (LHRF) heating is produced. The injected beam profile is moderated to produce the given the current and the pressure profile. Bootstrap current is also calculated in this code. With EQLAUS and ERATO, self-consistent MHD analysis can be investigate automatically.

2.3 0D system code and its validity

The use of the specialized code is consuming the time and the parameter survey is consuming the long time for the substantive results. 0D system code is used for quickly checking the basic criterion, such as the power balance, estimating the coil stress and making the radial build, before using the high-dimensional code.

The 0D system code, point model system code, is constructed that its physics and the engineering guideline is same as International Thermonuclear Experimental Reactor (ITER) Conceptual Design Activity (CDA) and Engineering Design Activity (EDA). The part of the estimation of the coil stress obeys the baseline of Fusion Experimental Reactor (FER) proposed at Japan Atomic Energy Research Institute (JAERI).

The 0D system code is constructed with referring the ITER CDA physics guidelines [49], the TORSAC code [20], and TRESCODE code [24]. Figure 2.3 is the flowchart of the 0D system code. The rest of this section, the detail relation of the plasma parameter calculation, TF coil design, CS coil design, bucking cylinder (BC) design, the radial build, and the neutron wall loading are described. Finally, the results (radial build) is compared with ITER EDA for the validity of 0D system code.

2.3.1 Basic plasma and coil analysis

Plasma analysis

The formulas described here are collected for ITER CDA [49], because almost all of these formulas were established with relatively high reliability based on the latest data

base in the fusion field.

The DT plasma is considered with major radius R, minor radius a, plasma elongation κ, and triangularity δ and it is assumed that the temperature of ions and electrons are same. The profile is assumed as,

$$X(r) = X(0)\left(1 - \frac{r^2}{a^2}\right)^{\alpha_x} , \tag{2.1}$$

for density n, current density j, and temperature T, with indices α_n, α_j, α_T, and where x_0 is the value at the plasma center. $\alpha_n \simeq 0.5$ and $\alpha_T \simeq 1.0$ is assumed in this thesis. The volume-averaged plasma power density is given by

$$\left\langle \frac{\partial W_{\rm th}}{\partial t} \right\rangle / V_{\rm p} = \langle P_{\rm OH} + P_\alpha - P_{\rm cond} - P_{\rm Br} - P_{\rm sync} + P_{\rm aux} \rangle / V_{\rm p} , \tag{2.2}$$

where W is plasma thermal energy, and $P_{\rm OH}$, P_α, $P_{\rm cond}$, $P_{\rm Br}$, $P_{\rm sync}$, $P_{\rm aux}$ are total powers of ohmic heating (OH), alpha particle heating, confinement loss, Bremsstrahlung radiation loss, synchrotron radiation loss and additional heating in MW, with plasma volume $V_{\rm p} = 2\pi^2\kappa a^2 R$. Details of these terms are given in Appendix D in the Ref. [49]. Effective plasma charge $Z_{\rm eff}$ is defined as,

$$Z_{\rm eff} = 1 + 2f_\alpha + Z(Z-1)f_{\rm Z} , \tag{2.3}$$

where f_α is alpha particle fraction of ion density defined by $f_\alpha = n_\alpha / n_{\rm e}$, Z is the charge number of impurity ion, and $f_{\rm Z}$ is the impurity ion fraction of ion density.

The energy confinement time τ_E is taken as follows [50],

$$\frac{1}{\tau_{\rm E}} = \left(\frac{1}{\tau_{\rm NA}^2} + \frac{1}{\tau_{\rm EH}^2}\right)^{1/2} , \tag{2.4}$$

where $\tau_{\rm NA}$ is Neo-Alcator OH confinement time [51]. $\tau_{\rm EH}$ is the energy confinement time for auxiliary heated plasmas. The Neo-Alcator confinement time takes the form

$$\tau_{\rm NA} = 0.07 n_{20} a R^2 q_* , \tag{2.5}$$

where $\langle n_{20} \rangle$ [$10^{20}\mathrm{m}^{-3}$] is the volume-averaged electron density, q_* is the cylindrical equivalent safety factor expressed by

$$q_* = \frac{5a^2 B_0}{R I_\mathrm{p}} \frac{1+\kappa^2(1+\delta^2-1.2\delta^3)}{2}, \tag{2.6}$$

where B_0 [T] is the toroidal field at the plasma center, I_p [MA] is total plasma current. For the energy confinement time of auxiliary heated plasmas, the enhanced ITER-89 power law scaling is adopted which is given by

$$\begin{aligned} \tau_\mathrm{EH} &\equiv f_\mathrm{H} * \tau_\mathrm{E}^\mathrm{ITER89\text{-}P} \\ &= f_\mathrm{H} * 0.048 A_\mathrm{i}^{0.5} I_\mathrm{p}^{0.85} R^{1.2} a^{0.3} \kappa^{0.5} \bar{n}_{20}^{0.1} B^{0.2} P_\mathrm{h}^{-0.5}, \end{aligned} \tag{2.7}$$

where f_H is the H-factor, the enhancement factor from the L-mode, A_i is the ionic mass number, and P_h [MW] is the total heating power defined by

$$P_\mathrm{h} = P_\mathrm{OH} + P_\alpha - P_\mathrm{cond} - P_\mathrm{Br} - P_\mathrm{sync} + P_\mathrm{aux}.$$

Greenwald density limit is defined as

$$\langle n_{20} \rangle_\mathrm{GR} = 0.27 \frac{I_\mathrm{p}}{a_\mathrm{p}^2}. \tag{2.8}$$

Plasma inductance is given by

$$L_\mathrm{p} = \mu_0 R \left(\ln \frac{8R}{\langle a \rangle} + \frac{l_\mathrm{i}}{2} - 2 \right), \tag{2.9}$$

where μ_0 is the vacuum permeability, $\langle a \rangle = a\kappa^{0.5}$ is the effective plasma radius, and l_i is the internal inductance of the plasma.

The loop voltage of the plasma becomes

$$V_\mathrm{loop} = 2.15 \times 10^{-3} \langle \gamma_\mathrm{NC} \rangle Z_\mathrm{eff} \frac{I_\mathrm{ind} R}{\kappa a^2} \langle T_{10} \rangle^{-3/2}, \tag{2.10}$$

where $\langle \gamma_\mathrm{NC} \rangle$ is the enhancement factor of the Spitzer resistivity due to the trapped particle effect given by

$$\langle \gamma_\mathrm{NC} \rangle = \frac{\left(\frac{1+\alpha_n}{1+\alpha_n+\alpha_T} \right)^{3/2}}{\int_0^1 dx\, 2x(1-x^2)^{3\alpha_T/2}(1-1.95\sqrt{\varepsilon x}+0.95\varepsilon x)}, \tag{2.11}$$

$\langle T_{10} \rangle$ [10 keV] is the volume-averaged temperature, I_ind [MA] is the inductively driven current defined as $I_\mathrm{ind} = I_\mathrm{p} - I_\mathrm{bs}$, and ε is the inverse aspect ratio.

The toroidal beta limit by Troyon scaling [52] is represented by

$$\beta_\mathrm{t}^\mathrm{max}\ [\%] = g \frac{I_\mathrm{p}}{a B_\mathrm{t}}, \qquad g = 2.5 \sim 3.5. \tag{2.12}$$

The ratio of the bootstrap current to the total plasma current f_bs is

$$f_\mathrm{bs} \equiv \frac{I_\mathrm{bs}}{I_\mathrm{tot}} = C_\mathrm{bs} (\varepsilon^{1/2} \beta_\mathrm{p})^{1.3}, \tag{2.13}$$

where

$$C_\mathrm{bs} = 1.32 - 0.235 \frac{q_\Psi(a)}{q(0)} + 0.0185 \left(\frac{q_\Psi(a)}{q(0)} \right)^2, \tag{2.14}$$

$$\beta_\mathrm{p} = \beta_\mathrm{t} \left(\frac{B_\mathrm{t}}{B_\mathrm{pa}} \right)^2, \quad B_\mathrm{pa} = \frac{I_\mathrm{tot}}{5\langle a \rangle}, \tag{2.15}$$

where q_0 is the safety factor at the plasma center and q_Ψ is the safety factor at 95% flux defined as

$$q_\Psi(a) = q^* f(\varepsilon),$$

where I_bs and I_tot are the bootstrap current and the total current, and

$$f(\varepsilon) \simeq \frac{1.17 - 0.65\varepsilon}{(1-\varepsilon^2)^2}.$$

Non-inductance current drive efficiency is generally defined as

$$\gamma_\mathrm{CD} = \frac{\langle n_\mathrm{e} \rangle I_\mathrm{p} R_\mathrm{p}}{P_\mathrm{CD}} (1 - f_\mathrm{bs}), \tag{2.16}$$

therefore, the density limit by γ_CD is

$$n_\mathrm{limit} = \frac{\gamma_\mathrm{CD} P_\mathrm{CD}}{I_\mathrm{p} R_\mathrm{p} (1 - f_\mathrm{bs})}. \tag{2.17}$$

The current drive efficiency of neutral beam injection (NBI) γ_NBI is described in Ref [49].

From Fig. 2.4 which shows the reactor geometry, the following relations are obtained. The available total flux of the center solenoid (CS) coil is

$$\Psi_\mathrm{tot} = 2 \cdot \pi \left(R - a - d - w_\mathrm{TF} - \frac{w_\mathrm{CS}}{2} \right)^2 B_\perp, \tag{2.18}$$

where d is the distance between the plasma and the toroidal field (TF) coils and w_{TF}, w_{CS} are the thickness of the TF and CS coils. The vertical field magnetized by the CS coil, represented by $B_\perp$, swings in both the positive and the negative directions. The stored energy in the CS coil is

$$W_{\mathrm{CS}} \approx \pi \left(R - a - d - w_{\mathrm{TF}} - \frac{w_{\mathrm{CS}}}{2}\right)^2 2\kappa(a+d)\frac{B_\perp^2}{2\mu_0} . \tag{2.19}$$

The stored energy in the TF coil is

$$W_{\mathrm{TF}} \approx 2\pi^2 R\kappa(a+d)^2 \frac{B_\perp^2}{2\mu_0} , \tag{2.20}$$

where the minor radius of the TF coil is chosen to be $a + d$, and the elongation is taken to be the same as that of the plasmas. The TF coil current density is given by

$$j_{\mathrm{TF}} = \frac{RB_\perp}{\mu_0 w_{\mathrm{TF}}(R - a - d - w_{\mathrm{TF}}/2)} . \tag{2.21}$$

The thickness of the TF and CS coil should be determined by two criteria. One is the current density of the superconducting coil, given by Eq. (2.21), where the critical current density is a function of the maximum field strength. The other is the mechanical stress due to the electromagnetic force, and this criterion is discussed in the rest of this sections.

Stress analysis

TF coil TF coil is approximated by the three-arc approximation. By the three-arc approximation, the center of each arc, (x_1, z_1), (x_2, z_2), (x_3, z_3), their radii, A_1, A_2, A_3, and their angle, θ_1, θ_2, θ_3 are determined automatically with giving either the first arc's angle θ_1 or the radius A_3. The in-plane electromagnetic forces such as hoop force F_{H}, centering forth F_{R} and vertical force F_{Z} are given as the following equations.

$$\begin{aligned} F_{\mathrm{H}} &= 2\left(\int_0^{\theta_1} \frac{\mu_0 N I^2 \cdot A_1 d\theta}{4\pi(x_1 + A_1\cos\theta)} + \int_{\theta_1}^{\theta_1+\theta_2} \frac{\mu_0 N I^2 \cdot A_2 d\theta}{4\pi(x_2 + A_2\cos\theta)} \right. \\ &\quad \left. + \int_{\theta_1+\theta_2}^{\pi} \frac{\mu_0 N I^2 \cdot A_3 d\theta}{4\pi(x_3 + A_3\cos\theta)}\right) + \frac{\mu_0 N I^2}{4\pi R_1} \times h_{\mathrm{Z}} , \end{aligned} \tag{2.22}$$

$$\begin{aligned} F_{\mathrm{R}} &= 2\left(\int_0^{\theta_1} \frac{\mu_0 N I^2 \cdot A_1 \cos\theta d\theta}{4\pi(x_1 + A_1\cos\theta)} + \int_{\theta_1}^{\theta_1+\theta_2} \frac{\mu_0 N I^2 \cdot A_2 \cos\theta d\theta}{4\pi(x_2 + A_2\cos\theta)} \right. \\ &\quad \left. + \int_{\theta_1+\theta_2}^{\pi} \frac{\mu_0 N I^2 \cdot A_3 \cos\theta d\theta}{4\pi(x_3 + A_3\cos\theta)}\right) + \frac{\mu_0 N I^2}{4\pi R_1} \times h_{\mathrm{Z}} , \end{aligned} \tag{2.23}$$

$$\begin{aligned} F_{\mathrm{Z}} &= \int_0^{\theta_1} \frac{\mu_0 N I^2 \cdot A_1 \sin\theta d\theta}{4\pi(x_1 + A_1\cos\theta)} + \int_{\theta_1}^{\theta_1+\theta_2} \frac{\mu_0 N I^2 \cdot A_2 \sin\theta d\theta}{4\pi(x_2 + A_2\cos\theta)} \\ &\quad + \int_{\theta_1+\theta_2}^{\pi} \frac{\mu_0 N I^2 \cdot A_3 \sin\theta d\theta}{4\pi(x_3 + A_3\cos\theta)} , \end{aligned} \tag{2.24}$$

where NI is the total ampere turns and N is the number of TF coils. The centering force and vertical force are also given in analytical form such as,

$$F_{\mathrm{R}} = 2\pi\left(R_1 + \frac{\Delta_{\mathrm{T}}}{2}\right)\frac{B_{\mathrm{Tmax}}^2}{2\mu_0 N} \quad [\mathrm{N/m}] , \tag{2.25}$$

$$F_{\mathrm{Z}} = \frac{\mu_0 N I^2}{4\pi} \ln\frac{R_2}{R_1} \quad [\mathrm{N}] . \tag{2.26}$$

On the other hand, overturning forced F_{Y} is defined as

$$F_{\mathrm{Y}} = B_\perp \times \frac{NI}{N} \quad [\mathrm{N/m}] , \tag{2.27}$$

where $B_\perp$ is used for the plasma stability.

TF coil case The following stress occur in the coil case and the bucking cylinder.

1. **Outer ring** The tensile stress due to the tension force and the bending stress due to the centering force at the upper and lower shoulders of inner leg.
2. **Inner ring** The tensile stress due to the tension force and the bending stress due to the out-of-plane force.
3. **Side plate** The tensile stress due to the tension force and the bending stress due to the out-of-plane force.
4. **Bucking cylinder** The compressive stress due to the centering force.

The principal stress of the coil case is shown in Fig. 2.5. The steel in the winding is not counted in the TF coil stress calculation.

The average in-plane stress by in-plane force is obtained by

$$\sigma_1 = K_0 \frac{F_Z}{A_{\mathrm{can}}}, \tag{2.28}$$

where A_{can} is the coil case cross sectional area. The bending stress of the outer ring by the centering force and overturning force are given by the following,

$$\sigma_{31}(\text{outer ring}) = K_1 \frac{F_R}{b} \left(\frac{b}{\Delta_{\mathrm{can1}}} \right)^2, \tag{2.29}$$

$$\sigma_{32}(\text{outer ring}) = K_2 \frac{F_Y}{2\Delta_{\mathrm{can1}}} \left(1 + \frac{\Delta_{\mathrm{TF}}}{4\Delta_{\mathrm{can1}}} \right), \tag{2.30}$$

where Δ_{can1} is the thickness of outer ring of the case and

$$b = 2 f_{\mathrm{ts}} R_1 \tan \frac{\pi}{N}. \tag{2.31}$$

The bending stress of the inner ring by overturning force is given by

$$\sigma_3(\text{inner ring}) = \frac{K_3 F_Y}{\Delta_{\mathrm{can2}}} \left(1 + \frac{\Delta_{\mathrm{TF}}}{8\Delta_{\mathrm{can2}}} \right), \tag{2.32}$$

where Δ_{can2} is the thickness of inner ring of the case and Δ_{TF} is the thickness of the conductor of TF coil in major radius direction.

The bending stress of the side plate by overturning force is given by

$$\sigma_3(\text{side plate}) = \frac{K_4 F_Y \Delta_{\mathrm{TF}}}{\Delta_{\mathrm{can3}}^2}, \tag{2.33}$$

where

$$\Delta_{\mathrm{can3}} = R_1 \tan \frac{\pi}{N} - \frac{b}{2}. \tag{2.34}$$

Criterion of stress intensity Table 2.1 is listed the data for the yield strength σ_y and the tensile strength σ_u of coil case materials. SUS316LN is used in this thesis.

An allowable stress intensity for the primary membrane stress, S_m, is given by

$$S_m = \min\left(\frac{2}{3}\sigma_y, \frac{1}{3}\sigma_u \right). \tag{2.35}$$

Construction on the stress intensity of TF coil case is set by

$$\sigma_{a,i} = \frac{1.5 \times S_m}{SF_i}, \tag{2.36}$$

where $i = 1, 2, 3$ represent the outer ring, the inner ring and side plate. SF_i shows the engineering safety factor. The coil case is determined to satisfy the following criteria;

$$\text{outer ring,} \quad \sigma_1 + \sigma_{31} - \sigma_{32} \leq \sigma_{a1}, \tag{2.37}$$

$$\text{inner ring,} \quad \sigma_3(\text{inner ring}) \leq \sigma_{a2}, \tag{2.38}$$

$$\text{side plate,} \quad \sigma_1 + \sigma_3(\text{side plate}) \leq \sigma_{a3}. \tag{2.39}$$

CS coil The CS coil designed to be self-supporting for the hoop forces. Namely the cross sectional area of the stainless steel conduit is chosen assuming that each turn in the CS coil would be locally self-supporting. The tensile stress of conduit materials by hoop force is then calculated by

$$\sigma = \frac{B_{\mathrm{Pmax}} j_P \cdot (R_{\mathrm{sol}} - \Delta_p)}{f}, \tag{2.40}$$

where R_{sol} is the outer radius of CS coil, Δ_p is the thickness of conductor and

$$f = \frac{\text{conduit area}}{\text{conductor area}}.$$

An allowable stress intensity for CS coil is given by

$$\sigma_{\mathrm{CS}} \leq \frac{S_m}{SF_{\mathrm{CS}}}, \tag{2.41}$$

where SF_{CS} is the safety factor of CS coil.

Bucking cylinder A bucking cylinder (BC) is mainly used for supporting the system over centering force. An average compressive stress of bucking cylinder is given by

$$\sigma_c(\text{Bucking cylinder}) = \frac{N F_R}{2\pi \Delta_{\mathrm{BC}}}, \tag{2.42}$$

where Δ_{BC} is the thickness of the BC. On the other hand, allowable stress of BC is given by

$$\sigma_{a,4} = \frac{S_m}{SF_4}, \tag{2.43}$$

and the allowable bucking stress of BC is given by

$$\sigma_{ca}(\text{Bucking Cylinder}) = \frac{E \times \Delta_{BC}^2}{12(1-\nu^2) \times R_{BC}^2}, \tag{2.44}$$

where E is Young's modulus and ν is Poisson's ratio. The thickness of the bucking cylinder is determined as

$$\sigma_c \leq \min(\sigma_{a4}, \sigma_{ca}). \tag{2.45}$$

2.3.2 Coil design

Inner radial build

The outer radius of CS coil, R_{sol}, is evaluated by the following equations, if a necessary volt second $\Delta\phi$ is given be the operation scenario.

$$\Delta\phi = 2B_{Pmax}(1 - f_{EQ}) \times \left(R_{sol}^2 - R_{sol} \cdot \Delta_p + \frac{\Delta_p^2}{3}\right), \tag{2.46}$$

$$B_{Pmax} = \alpha_P \gamma f_{PS} \mu_0 J_{pw} \Delta_p, \tag{2.47}$$

where B_{Pmax} and J_{pw} are an allowable maximum field and a maximum current density of the CS coil, which specified as design conditions. γ is a correction coefficient for the finiteness of the CS coil. f_{PS} is a space occupation ratio of the superconductor over the CS coil including support structures. α_P is a ripple correction factor for the discreteness in Z direction. f_{EQ} represent a fraction of the field reduction due to the divertor coil field on hybrid-type CS coil. f_{EQ} strongly depends on the plasma shape and the operation scenario. f_{EQ} is initially given in this code, R_{sol} is determined by the location of TF coil.

The thickness of TF coil is calculated from the following equation,

$$\frac{B_{Tmax}}{\alpha_T} = \frac{\mu_0 J_{tw} \cdot 2\pi f_{ts}(R_T + \Delta_T/2)\Delta_T}{2\pi(R_T + \Delta_T)}, \tag{2.48}$$

$$R_T = R_{sol} + \Delta_{gap} + \Delta_{BC} + \Delta_{can1}, \tag{2.49}$$

where B_{Tmax} and J_{tw} are an allowable maximum field and current density, which are specified as design condition. f_{ts} is the space factor of the conductor in the toroidal direction. α_T is the ripple correction factor due to the discreteness at the inner leg. Δ_{gap} is specified, Δ_{BC}, Δ_{can1} and Δ_{can2} are determined from the stress calculation.

The shield thickness Δ, the distance between TF coil and inner plasma edge, is specified as initial input data. It is necessary to calculate the thermal and neutron shield from the plasma to the coil in the future.

TF coil design

TF coil is designed after the calculation of plasma parameters. The criteria of TF coil design are,

1. to make the current density of the conductor of TF coil to the allowable current density.
2. to make the stress intensity in the case of the TF coil to the allowable stress intensity.

The thickness of TF coil Δ_{TF}, Δ_{can1}, Δ_{can2} and Δ_{can3} are calculated by the above criteria. The position of inner TF coil leg which is defined at the center of the conductor R_1, is also determined.

On the other hand, the position of the outer TF coil leg R_2, is determined by a constraint of the toroidal field ripple γ_r at the plasma surface $R_e = R_p + a_a$, *i.e.*,

$$\gamma_r = \beta \left\{ \frac{1}{(R_e/R_1)^n - 1} + \frac{1}{(R_2/R_e)^n - 1} \right\} \tag{2.50}$$

where β is correction coefficient and n is the number of TF coil [20].

CS coil design

CS coil is connected to TF coil, the outer radius of OH coil, R_{sol} is determined from the position of the inner TF coil leg. The thickness of CS coil d_{sol} and the current density

of CS coil j_{sol} are calculated the following equations to correspond the hoop stress and the allowable stress,

$$d_{\mathrm{sol}} = \frac{B_{\mathrm{Pmax}}^2}{B_{\mathrm{Pmax}}^2 + S_{\mathrm{m}}/SF_{\mathrm{OH}} \cdot \alpha_{\mathrm{P}}\gamma_{\mathrm{CS}} f_{\mathrm{PS}}\mu_0}, \tag{2.51}$$

$$j_{\mathrm{sol}} = \frac{B_{\mathrm{Pmax}}}{\alpha_{\mathrm{P}}\gamma_{\mathrm{CS}} f_{\mathrm{PS}}\mu_0 d_{\mathrm{sol}}}. \tag{2.52}$$

When j_{sol} is larger than the allowable current density, the design is calculated again with corresponding j_{sol} and the allowable current density. The design would be failed if d_{sol} is larger than R_{sol}.

Bucking cylinder design

Bucking cylinder is connected to CS coil, the outer radius of BC, R_{BC} is determined from the position of CS coil. The thickness of BC d_{BC} is determined as compressive stress is equal to the smaller one, the allowable stress and buckling stress. The design would be failed if d_{BC} is larger than R_{BC}.

2.3.3 Neutron wall loading

An neutron density produced by the fusion reaction is calculated from the mesh points of the poloidal cross section of the plasma. The elongation and Shafranov shift are considered in this calculation. The fusion reaction cross section $\langle \sigma v \rangle$ is given by

$$\langle \sigma v \rangle = \exp\left(a_1/T^r + a_2 + a_3 T + a_4 T^2 + a_5 T^3 + a_6 T^4\right), \tag{2.53}$$

where T[keV] is the temperature, $r = 0.2935$, $a_1 = -21.377692$, $a_2 = -25.204654$, $a_3 = -7.1013427 \times 10^{-2}$, $a_4 = 1.937545 \times 10^{-4}$, $a_5 = 4.0246592 \times 10^{-6}$, $a_6 = -3.9836572 \times 10^{-8}$ [53].

Figure 2.6 shows the explanation of the calculation of neutron wall load. The neutron wall loading n is defined as

$$n = \iiint d^3\boldsymbol{r}\, \frac{n(\boldsymbol{r})|\boldsymbol{n} \cdot \boldsymbol{u}|}{4\pi|\boldsymbol{r}|^2} \tag{2.54}$$

where $n(\boldsymbol{r})$ is neutron density at the point $\boldsymbol{r}$, $\boldsymbol{n}$ is a normal unit vector at the observe point on the plasma wall, $\boldsymbol{u}$ is a unit vector in the direction from the observe point to point $\boldsymbol{r}$. The contribution from the dead space is eliminated in this integration [39].

2.3.4 The validity of 0D system code

ITER EDA is simulated by this 0D system code with the parameter listed in Table 2.2 for validity of the system code. The position and the thickness of TF coil and CS coil are listed in Table 2.3. The result of the code has a good consistency with the data from ITER EDA. The result of this code by ITER EDA parameter, the elevation view, the ground view, radial build and neutron wall loading are shown in Fig. 2.7. The radial build and the cross section of TF coil is also show in Fig. 2.8.

Table 2.1: Yield strength and the tensile strength of the stainless steels.

	SUS304LN	SUS316LN
yield strength σ_y	765.2 MPa	861.2 MPa
tensile strength σ_u	1648.1 MPa	1378 MPa

Table 2.2: Parameters of 0D system code.

parameter	value	parameter	value
f_{EQ}	0.0	γ_{OH}	1.0
α_p	1.0	f_{PS}	0.70
J_{pw}	21.31	f	1.0
f_{TS}	0.70	γ_τ	0.02
γ	1.0	K_0	1.5
K_1	0.5	K_2	0.75
K_3	0.5	K_4	0.91
J_{pw}	21.31	SF_{OH}	1.2
SF_1	1.0	SF_2	1.0
SF_3	1.0	SF_4	3.0

Table 2.3: Comparison with the result of 0D system code and ITER EDA.

	radius of CS coil	thickness of CS coil	thickness of TF coil	inner radius of the outer TF coil
ITER EDA	2.0 m	0.8 m	1.25 m	13.3 m
system code	1.8 m	0.7 m	1.40 m	13.5 m

Figure 2.1: Schematic view of a tokamak.

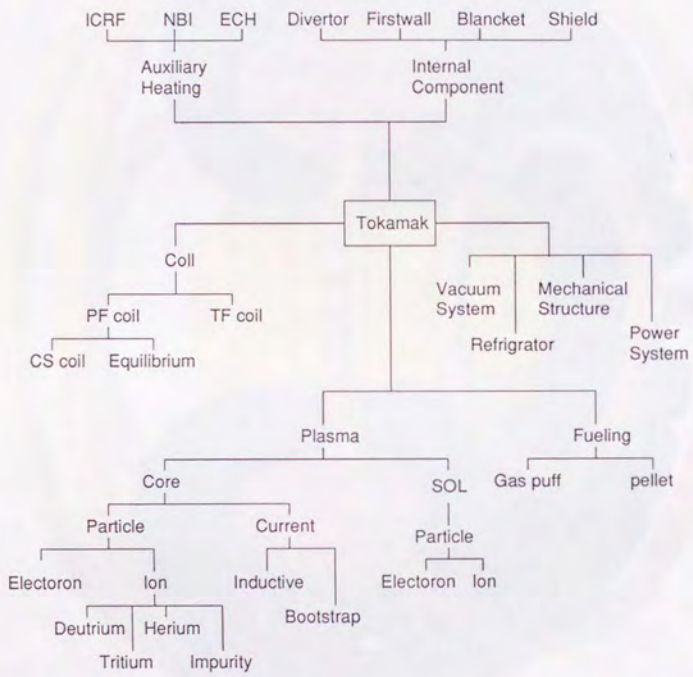

Figure 2.2: Tokamak as a complex system. The diagram of the components of the tokamak fusion reactor and its relation.

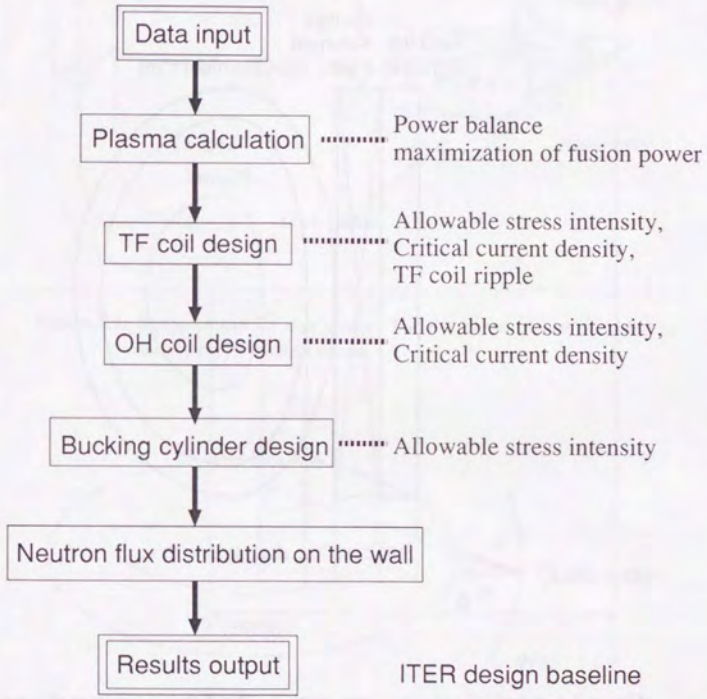

Figure 2.3: Flowchart of 0D system code. The design baseline of ITER is used in this code.

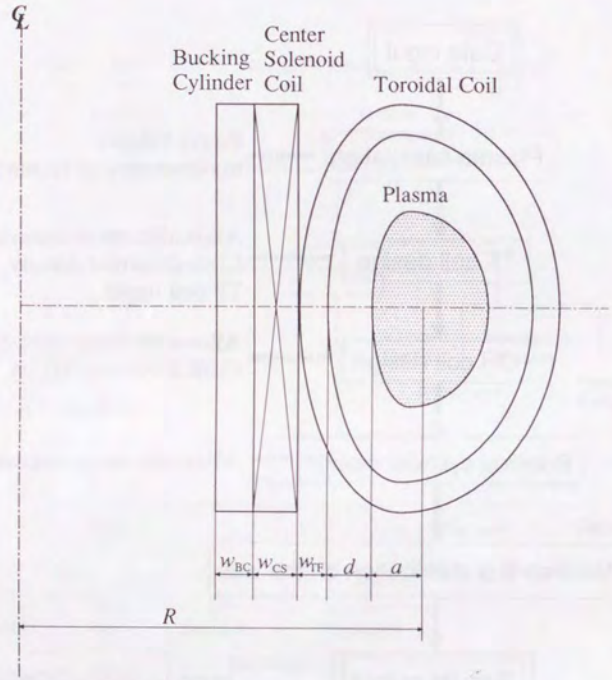

Figure 2.4: Schematic plasma cross section. The distance between plasma and TF coil is denoted by d, the thickness of the TF and CS coils are denoted by w_{TF} and w_{CS}, and the thickness of the BC is denoted by w_{BC}.

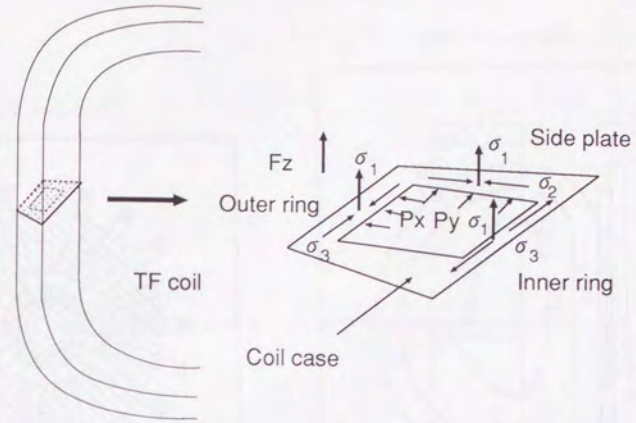

Figure 2.5: Stress of the TF coil's can. The thickness of can is varied to satisfy the allowable stress.

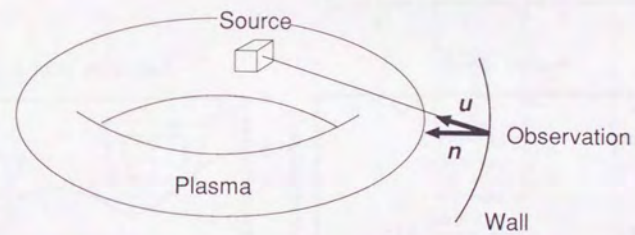

$\boldsymbol{n}$: normarized normal vector on the wall

$\boldsymbol{u}$: normarized vector to the source

$$N = \iiint dr^3 \frac{dn(r)\,|\boldsymbol{u}\cdot\boldsymbol{n}|}{4\pi|r|^2}$$

Figure 2.6: Distribution of the neutron wall load.

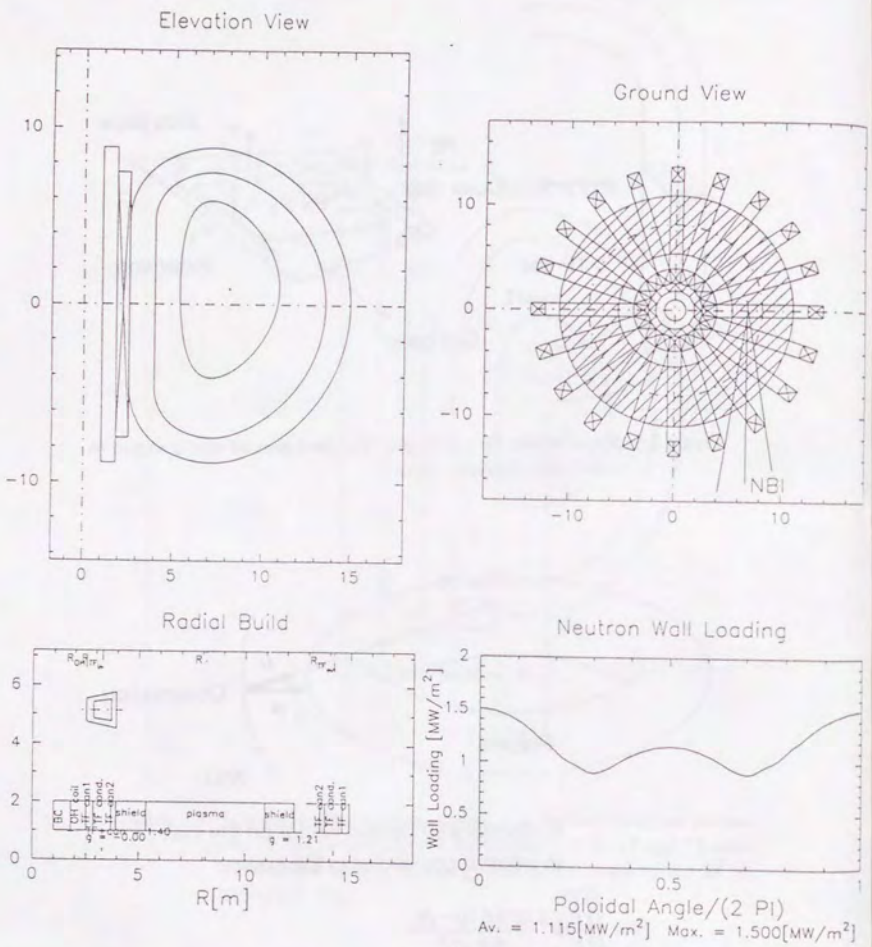

Figure 2.7: Results of the 0D system code, ITER EDA. The elevation view, the ground view, radial build and neutron wall loading are shown.

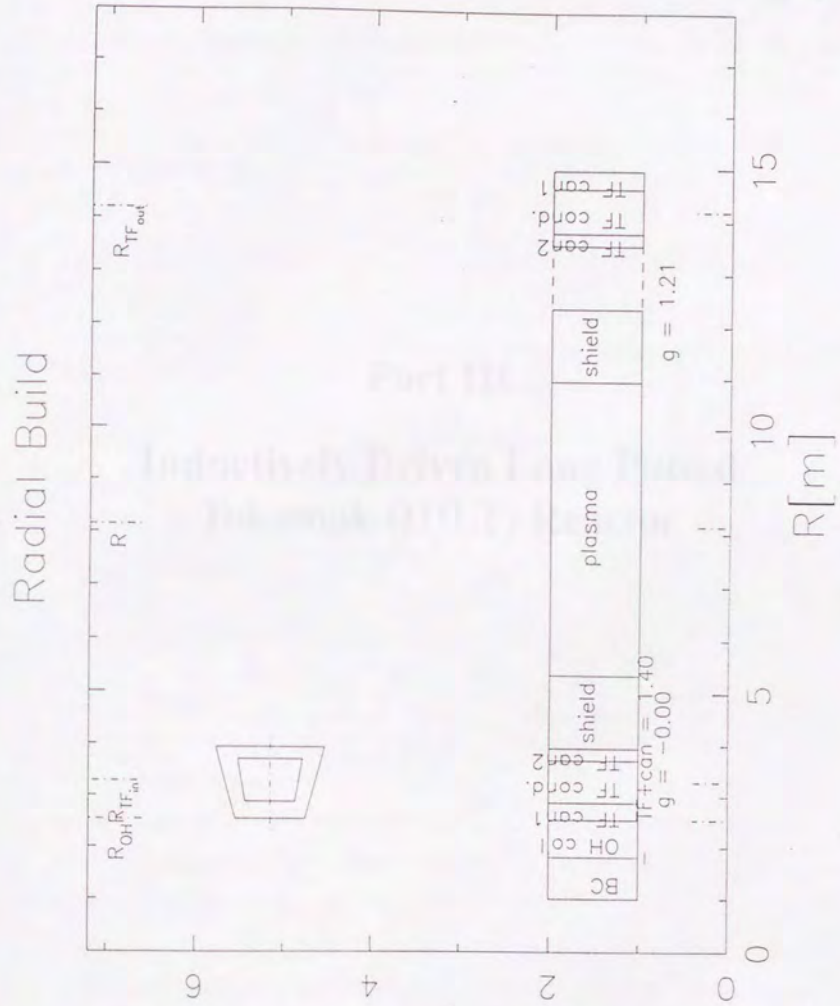

Figure 2.8: Radial build of ITER EDA by 0D system code.

Part III

Inductively Driven Long Pulsed Tokamak (IDLT) Reactor

Chapter 3

Introduction

3.1 Concepts of IDLT Reactor

The most experiment reactors are pulsed operated reactor because the plasma current is inductively current whose operation time is limited by magnetic flux of ohmic heating transformer. Recently, Inductively operated Day-Long Tokamak reactor (IDLT reactor) has been proposed [54].

3.1.1 Objectives of IDLT reactor

The principal objectives of IDLT reactor are ***"to realize the commercial fusion reactor as soon as possible in the conservative technology"*** and ***"to clarify a critical path to the realization of the fusion reactor through the discussions on merits and demerits of the pulsed reactor and the steady-state reactor."*** If ultimate goal of fusion reactor is steady-state reactor, many part of technology of long pulse reactor, such as IDLT reactor, could be used for its design and construction.

ITER project, the Concept Design Activity (CDA) phase, started on April 1988 and finished on December 1990, and the Engineering Design Activity (EDA) started on July 1992 and now continue its vitality activity in order to start the operation in 2004 and will terminate in 2020 [55]. As next step, DEMO reactor would be planned. Commercial reactor might be realized after the designing, the construction and the operation of DEMO

reactor. These scenarios come from avoidance of the risk, especially enormous physical and technical R&D.

The development of high efficiency current driven device is one of them. IDLT reactor does not use the current driven device for sustaining the plasma current but use it only during ramp up and down of the plasma current, therefore, IDLT reactor require lower output and shorter time of non-inductive current drive than that of steady state reactor. It may be possible for IDLT reactor to shorten the term of R&D.

The two essential problems related pulsed reactor, material thermal fatigue and compensation for electric output during re-charging transformer, are solved by very long pulsed operation. The discussion of this problems was described in Chapter 6.1.

3.1.2 Design baseline of IDLT reactor

The IDLT reactor design is based on the scientific knowledge from the operation of many tokamaks around the world over the past two decades and on the technical know-how following from the activity of ITER and Steady State Tokamak Reactor (SSTR) to substitute for the extensive technology R&D. The fusion performance of the plasma has been increased by two orders of magnitude in the last five years [55] and the technology is rapidly improved.

The design policies of IDLT reactor are

1. non-optimistic plasma physics and conservative technology are applied to approach the risk reduction. It is desired to need no or a few R&D programs for construction.
2. Pulse length is important but it would be restricted by the plasma physics and the technical issues.

These policies are come from objectives of IDLT reactor.

3.2 The series of IDLT reactor

3.2.1 The structure of this part

The series of IDLT reactor are consist of DEMO reactor, commercial reactor, and advanced commercial reactor. Each reactor is studied the following chapters. the summary and discussion of the series of IDLT reactor is described in Chapter 6.

DEMO reactor is designed as to produce the low fusion output and the low neutron wall loading. DEMO reactor would also produce the high fusion output, if materials tolerated for the high neutron fluence will be developed. The major radius is 10 m, the low fusion output is 0.8 GW and the high fusion output is 5 GW. In the case of the low fusion output, the early construction is possible because SUS316 can be used for the first wall which is also used ITER EDA. DEMO reactor is studied in Chapter 4.

The commercial reactor is the main reactor in this thesis. It is designed in the conventional plasma physics and the engineering or a little extrapolation from the state-of-art of technology. The dwell time is one of the problem for the continuous electrical output, so it should be short. the major radius is 10 m and the fusion output is 3 GW. The commercial reactor is studied in Chapter 5.

The advanced commercial reactor is also designed with the advance plasma physics such as H factor of 3 and the large bootstrap current ratio. The main purpose of this design is to compare the major radius between the conventional commercial reactor and advanced one. The major radius is 7.5 m, and the fusion output is 3 GW in the daytime and 1.5 GW at the night. The advanced commercial reactor is studied also in Chapter 5.

The pulsed reactor has two major disadvantage compared with the steady state reactor.

- Thermal and mechanical fatigue of structural materials caused by repeated operation.
- The electric power output of pulsed reactor is not constant.

The merits and the demerits of the pulsed reactor are discussed and summarized in Chapter 6.

3.2.2 Parameters of IDLT reactors

The birdview of early commercial IDLT reactor is shown in Fig. 3.1. It contains the thermal power regulation system which consists the hydrogen tank and boiler [56], and these devices is not necessary if power line grids accept the output of the pulsed operated reactor.

The principal parameter of IDLT reactors is shown in Table 3.1. IDLT reactor is high aspect machine, for enough volt-second of inductive transformer to sustain the plasma current. The plasma efficiency is improved with high elongation, however, vertical instability grow up. Toroidal field is limited under the restriction that maximum experience magnetic field of 13 T which is same as ITER EDA design. Plasma current I_p is determined by safety factor $q \propto 1/I_p$ to avoid the disruption.

Comparison plasma parameters with ITER EDA [57–63]), SSTR [64,65], ARIES-I [9] are listed in Table 3.2 [66]. The all of parameters of commercial IDLT reactor are listed in Table 3.3. The cross section of ITER, IDLT reactor, VNS, SSTR are shown in Fig. 3.2. VNS (Volumetric Neutron Source) is described in Appendix A.

Table 3.1: Principal parameters of the series of IDLT reactor.

parameter	DEMO	Commercial	Advanced
plasma major radius	10.0 m	10.0 m	7.5 m
plasma minor radius	2.9 m	1.85 m	1.85 m
elongation, 95% flux surface	1.5	1.7	1.7
maximum toroidal field	12.5 T	13 T	13 T
nominal plasma current	20.3 MA	12.4 MA	10.6 MA
nominal electrical output	0.24 GW	1 GW	1GW

Table 3.2: Comparison plasma parameters of IDLT reactor with other proposed reactor. Comm. and Adv. stand for commercial reactor and advanced commercial reactor, respectively.

	ITER (EDA)	IDLT DEMO	IDLT Comm.	IDLT Adv.	SSTR	ARIES-I
plasma major radius R [m]	7.7	10.0	10.0	7.5	7.0	6.75
plasma major radius a [m]	3.0	2.9	1.87	1.87	1.7	1.5
aspect ratio A	2.56	3.45	5.35	4.0	4.0	4.5
elongation κ	1.6	1.5	1.7	1.7	1.85	1.8
triangularity δ	~0.3	~0.3	~0.3	~0.3	~0.5	~0.2
plasma volume V [m^3]	2189	2490	1173	880	760	540
flux safety factor q_Ψ	~2.85	3.0	3.0	4.0	5.0	4.5
plasma current I_p [MA]	24	20.3	12.4	10.6	12.0	10.2
bootstrap current fraction	0.21	0.14	0.46	0.63	0.75	0.68
plasma temperature $\langle T \rangle$ [keV]	13	12	13	12	17	20
electron density $\langle n \rangle$ [10^{20}m^{-3}]	1.07	0.6	1.45	1.8	1.4	1.5
average toroidal beta β [%]	4.2	1.3	2.1	3.1	2.7	2.0
max. toroidal field $B_{t\,max}$ [T]	12.8	12.5	13	13	16.5	21
toroidal field on axis B_t [T]	5.7	7.12	8.75	7.33	9.0	11.3
heating/C. D. power [MW]	50	30	40	40	60	100
fusion power output [MW]	1500	800	2700	2700	3000	2544
power multiplication	~40	>500	>500	>500	50	~25
operation time	~0.28hrs	~4.5hrs	~7hrs	~6hrs	steady-state	steady state

Table 3.3: Parameter list of IDLT commercial reactor.

	IDLT Commercial
major radius R [m]	10.0
major radius a [m]	1.87
aspect ratio A	5.35
ellipticity κ	1.70
triangularity δ	~0.3
plasma volume V [m^3]	1173
max. toroidal field $B_{t\,max}$ [T]	13
toroidal field on axis B_t [T]	8.75
flux safety factor q_Ψ	3.0
plasma current I_p [MA]	12.4
bootstrap current fraction	0.46
He concentration f_{He} [%]	10
effective charge number Z_{eff}	1.5
average plasma temperature $\langle T \rangle$ [keV]	13
peak plasma temperature T_0 [keV]	22
average electron density $\langle n \rangle$ [10^{20}m^{-3}]	1.45
peak plasma density n_0 [10^{20}m^{-3}]	2.18
Greenwald density limit n_{Gr} [10^{20}m^{-3}]	0.96
Troyon factor g [%·m·T/MA]	2.8
average toroidal beta β_t [%]	2.1
average poloidal beta β_p	1.55
confinement enhancement factor f_H	1.80

continued on next page

continued from previous page

	IDLT Comm.
energy confinement time τ_E [s]	2.26
net electric output power P_{net} [MW]	1026
gross electric output power P_0 [MW]	1138
fusion power P_f [MW]	2700
thermal output power P_{th} [MW]	3348
power to SOL P_{SOL} [MW]	446
Bremsstrahlung power loss P_B [MW]	78
synchrotron rad. power loss P_s [MW]	26
synchrotron power loss recovery fraction	0.9
divertor heat flux P_{div} [MW/m^2]	26 $\sim$ 33
divertor temperature T_{div} [MW/m^2]	25 $\sim$ 60
inboard blanket-shield thickness [m]	1.4
OH coil field B_{OH} [T]	10
OH coil flux $2\Psi_{OH}$ [V·s]	1654
OH coil energy W_J [GJ]	46
TF coil energy W_t [GJ]	110
energy multiplication factor in blanket M	1.3
heat to electricity conversion efficiency η	0.34
plant efficiency η_{pl}	0.31
electric power fraction for plant operation ε	0.099
power for auxiliary systems P_{aux} [MW]	80
plasma heating power P_h [MW]	40(50)
heating duration [s]	40(30)

continued on next page

continued from previous page

	IDLT Comm.
fusion burning time t_b [hour]	7
dwell time t_{dw} [sec]	$\sim$ 600
current ramp up time t_u [s]	$\sim$ 40
current ramp down time t_d [s]	$\sim$120

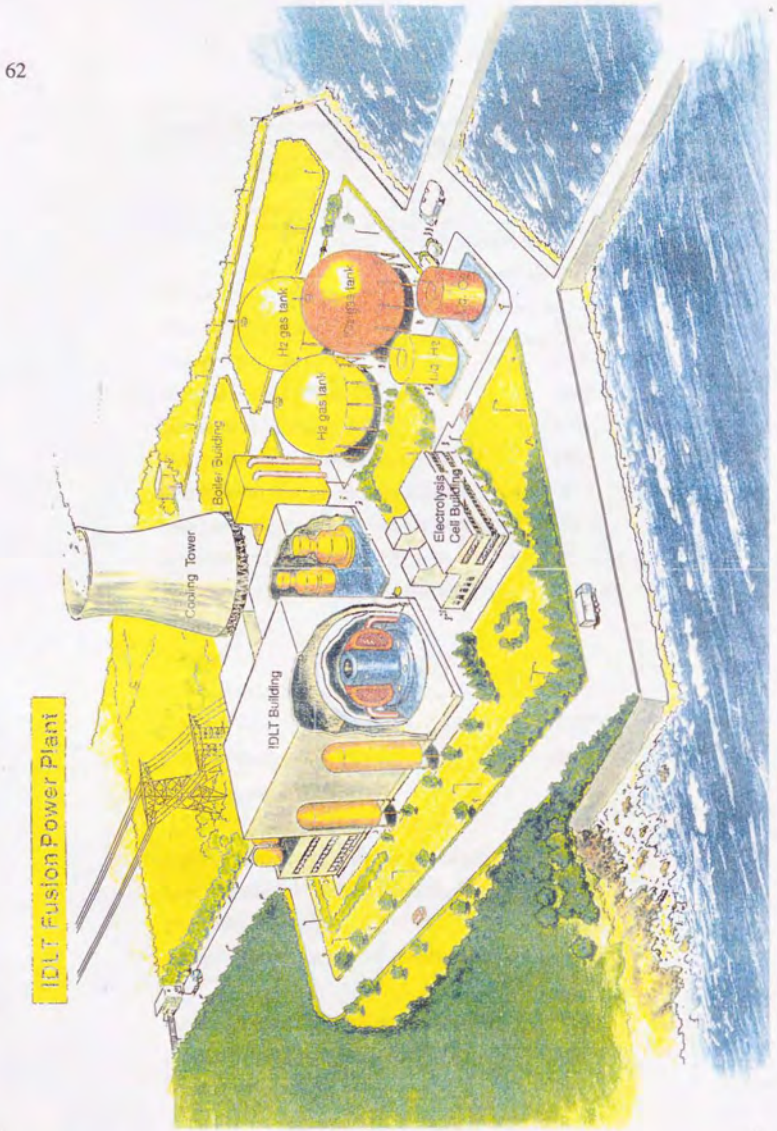

Figure 3.1: Birdview of IDLT reactor with power regulation system.

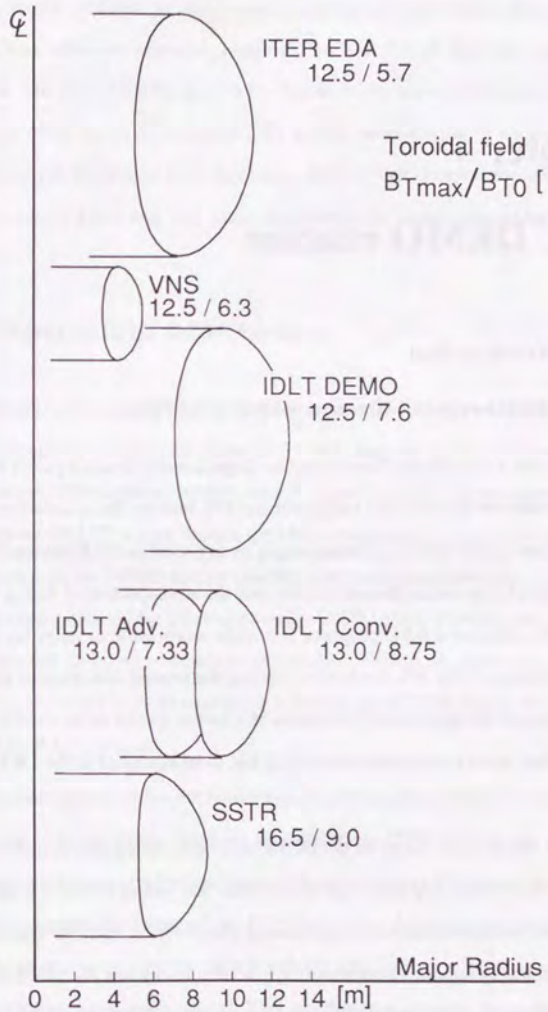

Figure 3.2: Cross section of ITER (EDA), IDLT Reactors, VNS and SSTR.

Chapter 4

IDLT DEMO reactor

4.1 Introduction

4.1.1 DEMO reactor, the next step from ITER

Recently, the International Thermonuclear Experimental Reactor called ITER is being designed under the international collaboration [67], and the demonstration of the scientific feasibility on DT ignition plasmas might be expected in ITER device. Based on this scientific knowledge on the plasma physics and the advancement of fusion nuclear engineering in the near-term R&D program, it is quite worthwhile to study on the feasibility of a DEMO reactor [68]. It is needless to say that the general definition of the DEMO is a demonstration of the engineering feasibility of a fusion reactor as an electric power plant, while detailed criteria and parameters which has to be equipped in the DEMO are not so clear.

Recently, the design activity on the DEMO has been started in U.S., where the general mission of the DEMO is clarified to demonstrate that fusion power is a secure, safe, licensable, and environmentally attractive power source that is ready for commercialization at an economically superior total cost [15]. While, Stacey has discussed on the DEMO from the viewpoint of the reasonable extension from the ITER, where two versions with conventional austenitic stainless steel and advanced vanadium alloys are designed for the DEMO [69].

So as to realize an attractive and economically-competitive fusion reactor, many R&D issues such as advanced material, high-field coils and high heat flux components are pointed out. For shortening the path to the fusion power plant, a pilot plant in advance of full-scale facilities has been proposed [70], where various types of tokamak plasma device are designed. In parallel with the design of the DEMO reactor, these R&D programs should be strongly promoted, and more attractive fusion reactor should be pursued.

4.1.2 Object of IDLT DEMO reactor

Our principal philosophy for the DEMO reactor is "***the early realization of the fusion reactor***", especially in the early phase of the next century and we believe that the construction of the DEMO reactor leads to launch a fusion energy into an argument on energy strategy. In our DEMO reactor design, therefore, the priority is given to the early and reliable realization of the DEMO reactor over the cost performance, because we should avoid optimistic expectation of the success on many R&D issues. Here we design the DEMO with the database based on presently-established knowledge on plasma physics and fusion engineering, most of which are employed in the design of ITER device and are planned in the near-term R&D program.

The schematic program for the fusion reactor development which we are proposing is shown in Fig. 4.1. Referring database available from ITER-BPP (Basic plasma performance) ignition plasma and Fusion Nuclear Testing, such as VNS described in Appendix A, we can complete the design of the DEMO reactor. After several-years' construction phase, we can start to operate the DEMO in 2023 with a full or a limited fusion power, depending on the material development. This development scenario is extrapolatable to the fusion commercial reactor such as commercial Inductively Driven Long pulsed Tokamak reactor called IDLT reactor described next chapter.

4.1.3 Review of the material for DEMO reactor

One of the most important R&D issues for fusion reactors is a development of the advanced materials such as ferritic steel, Vanadium, SiC and so on. SiC has a quite high tolerance for neutron irradiation, but engineering experience for the large-scale structural material seems to be quite premature. Vanadium alloy is a candidate for blanket materials on ITER EPP-phase, but the industrial application is quite poor, and the compatibility with coolant might be serious. The tolerance for neutron irradiation in ferritic steel might be acceptable in DEMO reactor, and the irradiation test for various types of ferritic steel is strongly promoted [71]. However, recent study on plasma disruption points out the requirement on the remarkable reduction of the error field ($\Delta B/B_0 = 10^{-4} \sim 10^{-5}$) [72]. The error field due to ferritic steel might be carefully taken into account, even though the ferritic steel is used in the magnetically saturated condition.

Characteristics of the austenitic stainless steel and its limitation for the advanced fusion systems are summarized in Ref. [73], where swelling resistance, radiation hardening, helium embrittlement, and irradiation assisted stress corrosion cracking (IASCC) seems to be main concerns, and the neutron fluence of $1 \sim 2$MW·a/m^2 seems to be an upper limit in fusion reactors. While, we have a plenty of experiences and achievements in fission reactors on the austenitic stainless steels, and the improved austenitic stainless steel tolerable up to $\sim$ 100 dpa (displacement per atom) has been developed in FBR as PNC1520 [74]. From these standpoints we believe that the earliest path to realize a DEMO reactor is the utilization of the austenitic stainless steel in the first stage. The long term of R&D of the material is not needed. To satisfy the design criterion for the austenitic stainless steel, the DEMO reactor has to be designed so that the ignition plasma is achievable even in a low fusion power, being sacrificed a slight increase of the plasma volume. Since this DEMO reactor has a capability to produce a further fusion power, a step-wise increase on the fusion power is possible, keeping in step with the material development.

4.1.4 The demand for the power supply on DEMO reactor

Other critical criterion of the DEMO reactor is an electric power supply in the range of a few hundreds MWe continuously (or intermittently) to the commercial network with high availability. The steady-state operation is preferable for continuous supply of the electric power, but the pulsed operation with a sufficiently high duty factor is not exclusive, because in DEMO reactor the continuous output of electric power to the commercial network is not indispensable.

According to above mentioned philosophy, we design the pulsed DEMO reactor, and discuss its performance and perspective as a test reactor for the developments on the advanced physics and technology.

4.2 Basic parameter design

4.2.1 Basic parameter decision

Calculation basis

Plasma design is based on the guideline proposed in ITER-CDA (Conceptual Design Activity) [49]. A plasma with a major radius R and a minor radius a is considered, and assume a profile of the plasma parameters with the form of $x(r) = x(0)(1-(r/a)^2)^{\alpha_x}$, where x denotes plasma density and temperature. Here we assume to be $\alpha_n = 0.5$ and $\alpha_T = 1$. The safety factor at the plasma surface $q_\Psi(a)$ is chosen to be 3. According to the increase of a plasma elongation κ and triangularity δ, the plasma performance such as plasma confinement and beta limit is improved, but the controllability for a vertical instability such as VDE(Vertical Displacement Event) and the compatibility with the divertor configuration become worse. In addition, in order to keep a stability for a highly elongation plasma such as ITER-CDA design (*e.g.*, $\kappa > 1.8 \sim 2$), the feedback coil interlinked with TF coil is required. While, in ITER-EDA design, the plasma elongation is remarkably reduced down

to $\kappa < 1.6$, and the triangularity of 0.24. As the aspect ratio is increased, the vertically elongated plasma becomes more unstable, resulting in the increase of the growth rate on the vertical instability. Taking this vertical stability criterion into account, we reduce the plasma elongation, as the aspect ratio is increased.

We employ ITER89-P scaling with a confinement enhancement factor H of 2, and take the beta limit given by Troyon scaling into account. The accumulation of helium ash strongly affects on the ignition condition, although the pumping efficiency through the divertor region is not so clear. In ITER-EDA design, the fraction of the helium in the core plasma is assumed to be 12.3% in ITER89-P scaling. We also adopt this value for the helium fraction. As a primary impurity we consider a beryllium, and assume to be $1 \sim 2\%$.

In general, there exist two operating points; one is in a high-density/low-temperature regime and another is in a low-density/high-temperature one. The former is preferable for the compatibility with the divertor plasma, however, the thermal instability is caused in this regime. Therefore, we select low-density/high-temperature operation point because of the thermal stability.

The maximum magnetic field strength of TF coil $B_{\mathrm{t,max}}$ and OH coil $B_{\mathrm{OH,max}}$ are selected to be 12.5 T and 13 T. The distance d_{pc} between the plasma surface and the TF coil position at the maximum magnetic field strength is assumed to be 1.4 m. The widths of TF coil w_{TF} and OH coil w_{OH} are determined by the mechanical stress and the current density of the superconducting coil with 0D system code described in Chapter 2. The toroidal field strength at the plasma center B_{t} and the available flux Φ_{OH} at the central solenoid are resultantly given by

$$B_{\mathrm{t}} = \frac{B_{\mathrm{t,max}}(R - a - d_{\mathrm{pc}})}{R}, \tag{4.1}$$

$$\Phi_{\mathrm{OH}} = 2B_{\mathrm{OH}}(R - a - d_{\mathrm{pc}} - w_{\mathrm{TF}} - w_{\mathrm{OH}}/2)^2. \tag{4.2}$$

The average neutron flux ψ_n and the maximum neutron flux are calculated by 0D system code.

Calculation results

The device size for satisfying an ignition condition is explored for various aspect-ratio plasmas. Figure 4.2 shows a critical fusion power necessary for igniting a plasma as a function of the major radius for various aspect-ratio plasmas. If we want to realize an ignition plasma with a smaller device, we have to increase the fusion power extremely, although the beta limit imposes the upper limit of the maximum fusion power. For example, in ITER-EDA plasma with the major radius of 8.1 m, the fusion power of 1.3 GW is indispensable for achieving an ignited plasma. However, this high fusion power yields other engineering problems such as handling of high heat flux at the divertor plate and developments of the first wall materials tolerable for the high neutron flux.

Here, we should pay attention that the critical fusion power is a very strong function of the major radius. In other words, a slight increase of the major radius yields a remarkable reduction of the critical fusion power. For example, if the major radius is increased from 8.1 m to 8.5 m, the critical fusion power becomes to be 0.6 GW. Although the cost of the device might increase with the major radius, the reduction of the fusion power would make it possible to adopt more established technology, and to guarantee a high reliability of the plant.

In Fig. 4.3 an average neutron wall loading is estimated for these parameters. The neutron flux of 1 MW/m^2 is expected in ITER-EDA. Here we set the design criterion on the neutron flux less than 0.5 MW/m^2. When a poloidal asymmetry of neutron flux is taken into account, the maximum neutron flux might become $0.8 \sim 1.0$ MW/m^2. Even if the austenitic stainless steel is employed in this DEMO reactor, replacement in every 2 – 3 years might be sufficient in the circumference for high duty factor of 50%.

Another requirement for the DEMO reactor is the operation period, when the pulsed mode operation is adopted. Figure 4.4 shows the operation period for each parameter. The dwell time of the inductively-operated tokamak is, roughly speaking, about 5 – 10 minutes. To realize a high availability of the DEMO reactor, the operation period of a few hours would be required. In the case of A = 2.7, it would be not available to design a device with a long operation period more than a few hours.

The construction for the long operation period up to 3 $\sim$ 4 hours requires the device with the aspect ratio of $A \sim 3.5$. From these consideration we have selected device parameters of DEMO reactor as follows; R = 10 m, a = 2.9 m (A = 3.45), P_{f} = 0.8 GW, ϕ_{n} = 0.4 MW/m^2, $\langle T \rangle$ = 12 keV and operation period of 4.5 hours. The cross section of DEMO reactor is depicted in Fig. 4.5, where all of the poloidal coils are located outside of the TF coils, and the sufficient space is prepared for the divertor room at the lower part of the vacuum chamber.

The POPCON plot of this DEMO reactor is shown in Fig. 4.6, where lines of P_{f} = 0.8 GW and Troyon g = 3 are also depicted. There exists two operation points; one is low-temperature/high-density regime ($\langle T \rangle$ = 8.7 keV, $\langle n_{20} \rangle$ = 0.84) and another is high-temperature/low-density regime ($\langle T \rangle$ = 12 keV, $\langle n_{20} \rangle$ = 0.6), and the operation periods are 2.7 hours and 4.5 hours. Since the latter is thermally stable, and give a long operation period, we select the high-temperature/low-density operation point.

Since this DEMO reactor is operated at the reduced power level with a Troyon factor g of 1.2, there exists a great margin for the beta limit. This gives an opportunity for this DEMO reactor to be operated at the elevated fusion power. Usually the maximum fusion power is limited by the Troyon factor. If the beta limit with the Troyon factor of 3 is acceptable, the fusion power of 5 GW is available in this DEMO reactor with an advanced neutron wall loading of 2.5 MW/m^2. The pulse length is prolonged up to 6 hours at the full power operation, because of increase of the bootstrap current fraction. Therefore, if the

materials tolerable for high neutron flux are developed, and high heat flux can be handled at the divertor region, this DEMO reactor is conceivable for high power fusion reactor. Parameters of the DEMO reactor is listed in Table 4.1 for limited and full power cases.

4.2.2 0D system code, the wall loading

0D system code is used the previous parameter survey, and Figure 4.7 shows the result of IDLT DEMO reactor. It shows elevation view, ground view, radial build, and the neutron wall loading. The neutron wall loading of IDLT DEMO reactor is lower than that of ITER EDA (Figure 4.8). The structure material for ITER EDA is SUS316 for the enormous experiment by fission reactor. Therefore, SUS316 is also used for IDLT reactor for the structure material.

4.3 Operating scenario

4.3.1 Ramp-up time

From the POPCON plot, in Fig. 4.6, the auxiliary heating of 20 MW would be enough to reach the self-ignition region, however, the investigation that how long the auxiliary heating turn on is necessary for IDLT DEMO reactor. The ramp-up simulation based on 0D power balance equation is calculated for determining the length of the auxiliary heating. The detail of the ramp-up simulation is described in the next chapter.

The calculation result is shown in Fig. 4.9. The auxiliary heating power of 20 MW is enough to enter the self-ignition region, however, it takes about more than 50 seconds. The heating time can be shorten by increase the heating power; The auxiliary heating of 25 MW and 30 MW, it takes about 40 and 30 seconds, respectively. The IDLT DEMO reactor adopt the auxiliary heating of 30 MW.